Heliyon 9 (2023) e19992

Contents lists available at ScienceDirect

Heliyon

journal homepage: www.cell.com/heliyon

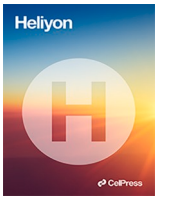

Review article

Chalcopyrite as an oxidants activator for organic pollutant remediation: A review of mechanisms, parameters, and future perspectives

Setareh Rostami- Javanroudi [a], Nazir Fattahi [a], Kiomars sharafi [a,b], Hossein Arfaeinia [c,d], Masoud Moradi [a,*]

[a] Research Center for Environmental Determinants of Health (RCEDH), Health Institute, Kermanshah University of Medical Sciences, Kermanshah, Iran
[b] Department of Environmental Health Engineering, School of Public Health, Kermanshah University of Medical Sciences, Kermanshah, Iran
[c] Systems Environmental Health and Energy Research Center, The Persian Gulf Biomedical Sciences Research Institute, Bushehr University of Medical Sciences, Bushehr, Iran
[d] Department of Environmental Health Engineering, Faculty of Health and Nutrition, Bushehr University of Medical Sciences, Bushehr, Iran

ARTICLE INFO

Keywords:
Chalcopyrite
Advanced oxidation processes
Persulfate
Peroxide
Organic pollutants
Degradation

ABSTRACT

Advanced oxidation processes (AOPs) based on oxidants have attracted attention for the degradation of organic pollutants. The combination of chalcopyrite with oxidants such as persulfate, peroxide, percarbonate, and others shows promise as a system due to its ability to activate through various pathways, leading to the formation of numerous radical and non-radical species. In this review, the generation of sulfate radical (SR) and hydroxyl radical (HR) in AOPs were summarized. The significance of chalcopyrite in various approaches including Fenton, photo-Fenton, and photo/Fenton-like methods, as well as its involvement in electrochemical Fenton-based processes was discussed. The stability and reusability, toxicity, catalyst mechanism, and effects of operational parameters (pH, catalyst dosage, and oxidant concentration) are evaluated in detail. The review also discusses the role of $Fe^{2+/3+}$, $Cu^{1+/2+}$, S^{2-} and S_n^{2-} present in $CuFeS_2$ in the generation of free radicals. Finally, guidelines for future research are presented in terms of future perspectives.

1. Introduction

Advanced oxidation processes (AOPs) are a promising approach to the oxidation of a broad range of organic pollutants [1]. AOPs through in situ generation of reactive oxygen species (ROS) lead to the complete mineralization of organic pollutants into water and carbon dioxide or transform refractory pollutants into biodegradable or less harmful intermediates [2–4]. Tursi A al have shown that AOPs are the removal approach that degraded pollutants via a non-selective way [5]. Nevertheless, the formation and release of nitro-products including nitrate, nitrite and ammonium ions during AOPs degradation of N-containing pollutants are one of the serious concerns of this process [6].

Previous studies suggested oxidants are the proper approaches for environmental remediation [7–9]. This is because oxidants offer

* Corresponding author.
E-mail address: mahfooz60@gmail.com (M. Moradi).

https://doi.org/10.1016/j.heliyon.2023.e19992
Received 18 June 2023; Received in revised form 6 September 2023; Accepted 7 September 2023
Available online 9 September 2023

distinct advantages within AOPs. Briefly, advantages of AOPs-based hydrogen peroxide and persulfate include efficient decomposition of a wide range of pollutants (especially refractory pollutants), generation of non-selective and selective oxidizing species (hydroxyl and persulfate radicals), flexibility in operation, low-cost and production of lower damaging by-products, accessibility and possibility for large-scale treatment applications [10–13].

For AOPs-based percarbonate, advantages include the safe and cost-effective alternative to H_2O_2, non-acidification of treated environments and the ability to operate in a wide pH range, possibility to generate various ROS, including superoxide and carbonate radicals which carbonate radicals although have lower the oxidation potential (1.78 V at pH 7) compared to the hydroxyl radical, they selectively react with organic pollutants containing electron-rich functional groups [14]. Therefore, AOPs based on the oxidants activation (peroxide (H_2O_2), persulfate (PS), percarbonate ($Na_2CO_3{\cdot}1.5H_2O_2$), etc.) have attracted high attention. This is primarily due to their flexibility, cost-effectiveness, and high efficiency as remediation technologies. These oxidants can be activated using various methods and activators, including ultraviolet irradiation, heat, carbon materials, microwave, ultrasound, catalyst-free systems, and transition metals [15–18]. However, the application of some activators may be limited due to various factors. These factors can include high energy, low activation capability, pH-adjustment before and after reaction and complexity of operation [19]. Meanwhile, the activation of oxidants through catalysts containing transition metals for the generation of reactive oxygen species (ROS) has been extensively employed in the degradation of pollutants [11]. Because transition metals are highly valuable and preferred options as oxidant activators in AOPs due to their high yield ROS generation, proper catalytic activity, reusability, applicability as homogeneously and heterogeneously, presence in natural catalysts, energy-saving, and cost-effectiveness [20,21]. Different transition metals including Ag, Ce, Fe, Cu, Co, Mn and etc. Have been used for the activation of PS, H_2O_2, and $Na_2CO_3.1.5H_2O_2$. Previous studies have demonstrated that the combination of transition metals to form bimetal catalysts, such as Cu/Fe, Co/Fe, and others, can significantly enhance oxidant activation. This improvement is attributed to the synergistic effects that arise from the interaction between the active sites of the bimetal catalyst [22–25]. Among the transition metals, Fe and Cu widely used for oxidant activation due to easy access, low adverse effect on the environment, and high catalytic activity, while the usage of certain transition metals such as silver (Ag) and cerium (Ce) is more restricted. This is primarily due to their higher cost and challenges in practical application [26,27]. Weng H et al. (2023) has reported that a Fe-containing catalyst is a promising approach in AOPs due to excellent adsorption and catalytic performance [28]. Chalcopyrite (CuFeS2) is a mineral that contains both copper (Cu) and iron (Fe) sulfide. It has gained attention as a potential "green catalyst" due to its ability to serve as a source of Cu and Fe sulfide in AOPs [29,30]. $CuFeS_2$ due to the existence of mixed valence of Cu and Fe facilitates greatly effective electron transfer on its surface. The following reactions (Eqs. (1)–(11)) can occur by $CuFeS_2$ in Fenton-based AOPs [29]:

$$CuFeS_2(s) + 8H_2O_2 \rightarrow Fe^{3+} + Cu^{2+} + 2SO_4^{2-} + 8H_2O + 2H^+ \quad (1)$$

$$CuFeS_2(s) + 16Fe^{3+} + 8H_2O \rightarrow 17Fe^{2+} + Cu^{2+} + 2SO_4^{2-} + 16H^+ \quad (2)$$

$$CuFeS_2(s) + 4O_2 \rightarrow Fe^{2+} + Cu^{2+} + 2SO_4^{2-} \quad (3)$$

$$CuFeS_2(s) + 4O_2 + 4H^+ \rightarrow Fe^{2+} + Cu^{2+} + 2S^0(s) + 2H_2O \quad (4)$$

$$CuFeS_2(s) \rightarrow Fe^{2+} + Cu^{2+} + 2S^0(s) + 3e \quad (5)$$

$$S^0(s) + 2H_2O + 3O_2 \rightarrow 2SO_4^{2-} + 4H^+ \quad (6)$$

$$Fe^{2+} + H_2O_2 \rightarrow Fe^{3+} + OH^- + OH^\bullet \quad (7)$$

$$Cu^{2+} + H_2O_2 \rightarrow Cu^+ + O_2^{\bullet-} + 2H^+ \quad (8)$$

$$Cu^+ + H_2O_2 \rightarrow Cu^{2+} + OH^- + OH^\bullet \quad (9)$$

$$Fe^{3+} + H_2O \rightarrow Fe(OH)^{2+} + H^+ \quad (10)$$

$$Fe(OH)^{2+} + h\vartheta \rightarrow Fe^{2+} + OH^\bullet \quad (11)$$

Copper present in chalcopyrite through reaction with oxidants (e.g.PS, H_2O_2) can induce the formation of different ROS including $^\bullet$OH, $SO_4^{\bullet-}$, $SO_5^{\bullet-}$, $O_2^{\bullet-}$ and non-radicals such as Cu^{3+}, $^1O_2$ and surface activated PS [31–33]. Cu ions principally occur in the state of Cu^+, Cu^{2+}, and Cu^{3+}. Since Cu^+ is unstable and simply can be disproportioned to zero-valent copper (Cu^0) and Cu^{2+}. Cu^+ could be stable through reaction with organic/inorganic. In contrast, Cu^{3+} plays the role of a potent oxidant within the medium. Consequently, in an aqueous solution, Cu^{3+} can undergo reduction to Cu^{2+} through reactions with hydroxyl ions, water molecules, and certain organic compounds. As Cu^{2+} demonstrates greater stability in the medium, it serves as the primary copper salt for activating the oxidant [19]. The main advantage of $CuFeS_2$ is releasing of Cu^{2+} and Fe^{2+} ions in an aqueous solution (Eqs. (2)–(5)) and self-regulation of solution pH [30]. Fe as the abundant and non-toxic material is the long-time activator for different oxidant in homogenous and heterogeneous types [34].

Different Fe-based materials including ferrous salts, ferric salts, zero-valent iron (ZVI), iron oxides, and iron sulfides have been applied to oxidants activation in order to decontaminate organic pollutants. The widespread utilization of Fe-based oxidant activators

can be attributed not only to their high efficacy but also to their cost-effectiveness and eco-friendliness [35]. Ferrous is one of the most widely used iron salts in AOPs. The use of this activator in AOPs presents certain drawbacks. These include the requirement for high acidic pH values (2.8–3.5), low reuse, sludge production, and quenching effect at high dosages. Therefore, a solid catalyst containing iron is the proper approach to resolve this drawback [36]. Chalcopyrite also through the release of Fe^{3+}, Cu^{2+} and Cu^{+} ions, surface structure, and crystal defects provides the complex metal oxidation in AOPs such as photocatalytic and Fenton-like processes [37,38]. To the best of our knowledge, no comprehensive review has been conducted on the activation mechanism of various oxidants, including hydrogen peroxide, persulfate, and bicarbonate, using chalcopyrite as a mediator. Therefore, in the present study, we explore the mechanisms involved in the activation of oxidants, the generation of active radicals, the factors that influence their production, and the impact of chalcopyrite type (natural or synthesized) and synthesis methods on the efficiency of the process. as well as the effect of key operating parameters (pH, catalyst dosage, oxidant concentration and so on) to decompose organic pollutants has been evaluated in detail. Moreover, chalcopyrite synthesized and characterization, the mechanism of oxidant activation, stability and reusability, toxicity and ROS involved in various AOPs types including photocatalyst, electro-catalyst, Fenton, photo- Fenton, PS oxidation and etc. Have been evaluated.

2. Preparation of natural and synthesized chalcopyrite

Chalcopyrite in both natural and synthesized types has been applied for AOPs. The natural chalcopyrite type is mined from mines. In order to address the presence of impurities and pollutants in natural chalcopyrite, it is necessary to prepare the catalyst through specific processes. Milling and sieving were used in order to produce of powdered catalyst. To remove impurities and pollutants from the obtained powdered catalyst, several main steps including sonication of the powder in ethanol (95%), washing with nitric acid, and drying were used [30,39,40]. The evaluation of studies showed three approaches including hydrothermal, co-precipitation, and microwave-assisted hydrothermal have been used for the synthesis of chalcopyrite. Chalcopyrite is synthesized from a combination of compounds containing copper, iron, and sulfur. Studies have frequently used copper (I) chloride (CuCl), and ferric chloride ($FeCl_3$) as a source of Cu and Fe. In the synthesis procedure for preparing $CuFeS_2$, various compounds containing the element sulfur (S) were utilized as a source of sulfur. Wen PY et al. (2022) have synthesized the $CuFeS_2$ via hydrothermal and co-precipitation methods. In the hydrothermal route, they used the CuCl, $FeCl_3.6H_2O$ and sodium sulfide nonahydrate ($Na_2S.9H_2O$) as a source of sulfur. For this aim, certain amount of CuCl and $FeCl_3.6H_2O$ were added to the deionized water (DW) and then $Na_2S.9H_2O$ was dropwise added. Finally, the mixture was transferred into the Teflon-lined stainless-steel autoclave and heated at 200 °C for 10 h. In the co-precipitation method, a specific amount of CuCl and $FeCl_3.6H_2O$ were added to the DW and stirred at 70 °C for 10 min. Subsequently, ammonium (30%) and hydrazine hydrate (64–65%) were added to the mixture. Then the $Na_2S.9H_2O$ was added to the mixture and stirred at 70 °C for 3 h [29]. Vieira Y et al. (2022) synthesized chalcopyrite similar to Wen PY's study, with the difference that this work used cupric chloride ($CuCl_2$) as the Cu source and polyvinyl-pyrrolidone surfactant to balance electrostatic charges and provide promising conditions for gaining the favorite product [41]. Nie W et al. (2019) and Xu X et al. (2019) have synthesized $CuFeS_2$ via hydrothermal technique,

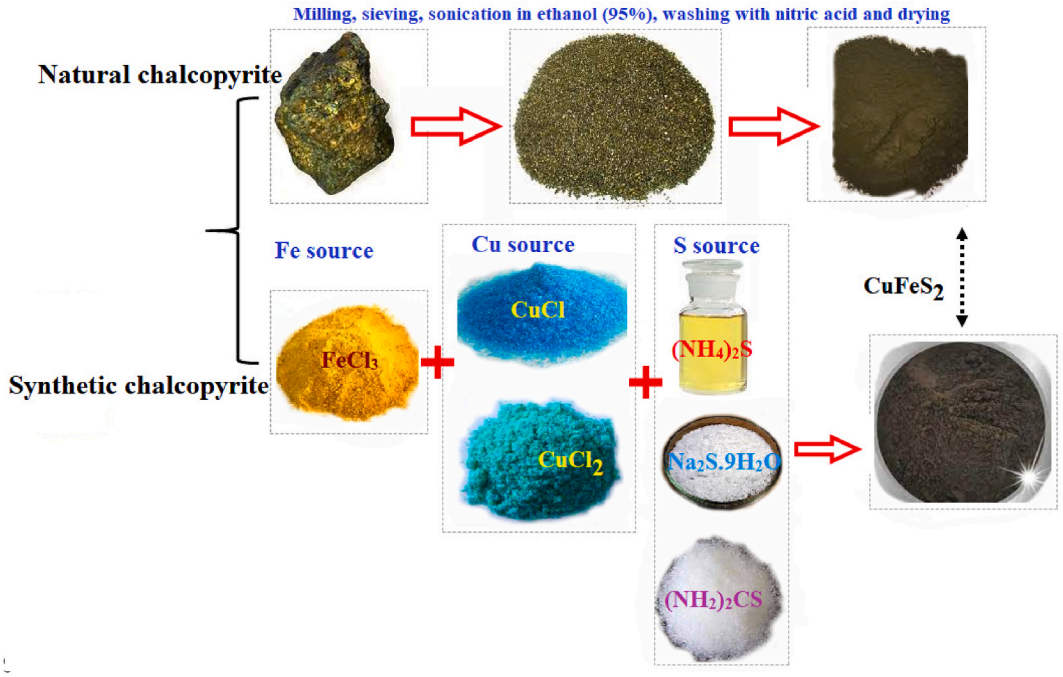

Fig. 1. The procedures synthesis of natural and synthetic chalcopyrite.

using materials including CuCl, $FeCl_3$, and ammonium sulfide $(NH_4)_2S$ as a sulfur source [37,42]. Considering the studies, only the source of sulfur is different in the synthesis of chalcopyrite and the source of copper and iron are the same. In the microwave-assisted hydrothermal method for $CuFeS_2$ synthesis, da Silveira Salla et al. (2020) were used CuCl, $FeCl_3.6H_2O$ and thiourea ($(NH_2)_2CS$) as a sulfur source. In this procedure, a certain amount of CuCl, $FeCl_3.6H_2O$, citric acid ($C_6H_8O_7$) and $(NH_2)_2CS$ were added to the DW and then irritated with microwave (1400 W and 7 min) until the temperature reached 200 °C [43,44]. In the cyclic microwave heating method for $CuFeS_2$ preparation, CuCl, $FeCl_3$, and L-cysteine compounds are utilized. In this method, the mentioned compounds were added to the DW and then irradiated with underwent 10 cycles of 36 s heating and a 36 s pause in a domestic microwave oven (Fig. 1) [45].

3. Summary of sulfate radical (SR) generation in AOPs

The chemical materials content of PS including PDS ($S_2O_8^{2-}$) and PMS (SO_5^{2-}) are the main sources of SRs [46]. Some advantages of PS based AOPs include high oxidation potential, long half-life, selective oxidation capacity and superior oxidation capability over a wide pH range [47]. The common characteristic of these compounds is the O–O bond. These compounds have some differences in chemical properties [48]. a) The O–O bond distance for PDS and PMS is f 1.453 Å and f 1.497 Å respectively b) The PDS is more stable than PMS due to the substitution of two individual hydrogen atoms of H_2O_2 by SO_3. c) The redox potential of PDS (2.01 V) is more than PMS (1.77 V) [49] d) PDS is the peroxide group that bridges two sulfur atoms, whereas PMS is a type of an S-inorganic hydroperoxide. Moreover, PMS could not be activated due to the presence of two "dead" sulfate salts in the molecular structure [48,50]. The activation of the PDS and PMS can break the O–O bond through homolytic or heterolytic cleavage, as a result, induces SRs generation [48]. Overall, both PDS and PMS bind to catalyst surfaces to form active complexes and react with pollutants, but there is ongoing debate about the differences and similarities in their reaction mechanisms [51].

Different approaches have been used for PDS and PMS activation including physical activation (heating, ultraviolet (UV), ultrasound (US)), and chemical activation (alkaline activation (Eq. (12)), transition metal ions, carbon-based materials). The mechanism of SRs generation by heating and UV is O–O bond fission (Eqs (13) and (14)). The energy input for PS/PMS activation by heating is 140.0–213.3 kJ/moL (>50 °C). Since the energy of O–O bond in PMS is more than PDS, the efficiency of the heat-activated PMS is lower than that of PDS [52]. Nevertheless, the generated SRs will be converted to hydroxyl radicals; as a result, pH will decrease in the continuation of the process (Eq. (15)). For ultrasound approach, in addition to the O–O bond fission, the hydrolysis of water molecules is also involved (Eqs. (16) and (17)). Also, the cavitation bubbles will be produced that induce high temperatures (i.e., 5000 K) and high pressure (i.e., 10 atm) [53,54]. This process causes SRs generation via homolysis of the O–O bond. However, the yield of $^{\bullet}OH$ is more than that of SR under US activation due to decomposition of H_2O molecules by cavitation bubbles [55,56]. Furthermore, the recombination rate of •OH may be halted at high temperatures, resulting in their concentration reaching mM level (Eq. (18)).

$$2S_2O_8^{2-} + 4OH^{\pm} \rightarrow O_2^{\bullet -} + SO_4^{\bullet -} + 3SO_4^{2-} + 2H_2O \quad (12)$$

$$S_2O_8^{2-} + \text{heat} \,/\, \text{UV} \rightarrow 2SO_4^{\bullet -} \quad (13)$$

$$HSO_5^{-} + \text{heat} \,/\, \text{UV} \rightarrow SO_4^{\bullet -} + HO^{\bullet} \quad (14)$$

$$SO_4^{\bullet -} + H_2O \rightarrow SO_4^{2-} + H^{+} + HO^{\bullet} \quad (15)$$

$$S_2O_8^{2-} + 2H_2O \xrightarrow{OH^{-}\,(US)} HO_2^{-} + 2SO_4^{\bullet -} + 3H^{+} \quad (16)$$

$$S_2O_8^{2-} + 2HO_2^{-} \xrightarrow{(US)} SO_4^{\bullet -} + SO_4^{2-} + H^{+} + O_2^{\bullet -} \quad (17)$$

$$H_2O \xrightarrow{(US)} H^{\bullet} + HO^{\bullet} \quad (18)$$

in the alkaline approach, the activation mechanism involves the hydrolysis of PS and PMS, leading to the formation of hydrogen

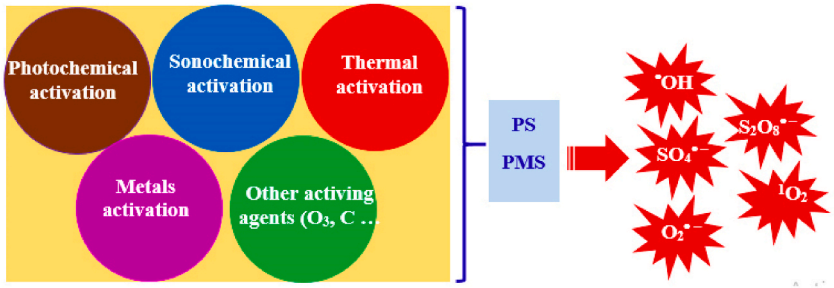

Fig. 2. Approaches used for SR generation.

peroxide (Eqs. (19)–(23)). On the other hand, for transition metal ions and carbon-based materials, the activation mechanism relies on single electron transfer (Eqs.(24)–(28)) (Fig. 2).

$$S_2O_8^{2-} + H_2O \rightarrow HO_2^{\bullet -} + 2SO_4^{-} + H^+ \quad (19)$$

$$S_2O_8^{2-} + HO_2^{-} \rightarrow SO_4^{\bullet -} + SO_4^{2-} + H^+ + O_2^{\bullet -} \rightarrow \rightarrow {}^1O_2 \quad (20)$$

$$HSO_5^{-} \rightarrow SO_5^{2-} + H^+ \quad (21)$$

$$HSO_5^{-} + H_2O \rightarrow HSO_4^{-} + H_2O_2 \rightarrow \rightarrow \rightarrow HO^{\bullet} + SO_4^{\bullet -} + O_2^{\bullet -} + {}^1O_2 \quad (22)$$

$$S_2O_8^{2-} + M^{n+} \rightarrow M^{n+1} + SO_4^{2-} + SO_4^{\bullet -} \quad (23)$$

$$HSO_5^{-} + M^{n+} \rightarrow M^{n+1} + OH^{-} + SO_4^{\bullet -} \quad (24)$$

$$S_2O_8^{2-} + ACsurface - OOH \rightarrow SO_4^{\bullet -} + Csurface - OO^{\bullet} + HSO_4^{-} \quad (25)$$

$$S_2O_8^{2-} + ACsurface - OH \rightarrow SO_4^{\bullet -} + Csurface - O^{\bullet} + HSO_4^{-} \quad (26)$$

$$HSO_5^{-} + C - \pi \rightarrow C - \pi^+ + SO_4^{\bullet -} + OH^{-} \quad (27)$$

$$HSO_5^{-} + C - \pi^+ \rightarrow C - \pi + SO_5^{\bullet -} + H^+ \quad (28)$$

4. Summary of hydroxyl radical (HR) generation in AOPs

HR is the reactive oxygen species which widely used as a potent oxidizing agent for organic contaminants degradation. The oxidation potential of HR is between 2.8 V (pH = 0) and 1.95 V (pH = 14). The constant rate of HR in reaction with the target pollutant is 10^8–10^{10} M^{-1} s^{-1}. Radical addition, hydrogen abstraction, electron transfer, and radical combination are the main ways for pollutant degradation by HR. The principal features of HRs include their non-selectivity, short lifetime, in situ generations and rapid reaction with organic matter [57]. Different approaches including gamma ray/electron beam radiation, photochemical oxidation, photocatalysis, sonolysis, Fenton-based reactions, and ozone-based processes have been used for HRs generation [58]. Gamma-ray/electron beam radiation is one of the applied technologies for the resolution of the problems of the different environmental fields. The combination of metal oxides such as TiO_2 with UV/oxidants (UV/H_2O_2, UV/O_3, UV/O_3/H_2O_2) has been proposed as an effective approach for generating HR in AOPs. This combination leads to improving the efficiency and effectiveness of AOPs due to the synergistic effect on the production of HR. Because metal oxides act as catalysts, while UV/oxidants provide the necessary energy and reactive species to initiate and maintain the HR production process [33,59]. The $^{\bullet}OH$, $^{\bullet}H$ and hydrated e^- radicals could be generated under light irradiation. The hydrated e^- and $^{\bullet}H$ finally react with O_2 and produced the $O_2^{\bullet -}$ and $HO_2^{\bullet -}$ (Eqs.(29)–(31)).

$$H_2O \rightarrow HO^{\bullet} + H^{\bullet} + e_{aq}^{-} + H_2O_2 + H_2 \quad (29)$$

$$e_{aq}^{-} + O_2 \rightarrow O_2^{\bullet -} \quad (30)$$

$$H^{\bullet} + O_2 \rightarrow HO_2^{\bullet -} \quad (31)$$

In photochemical oxidation, according to the type of oxidant used, different radicals are produced. The HRs is the main ROSs when hydrogen peroxide is used as oxidant (Eq. (32)). The photocatalyst approach is the most attractive way in order to HRs generation. In this approach, the photo-induced electron (e_{CB}^-) and electron-hole (h_{vB}^+) can be generated in the catalyst [60]. HRs could be generated due to e_{CB}^- and h_{vB}^+ reactions with the hydroxyl ions and water molecules (Eqs.(32)–(35)) [61,62].

$$H_2O_2 + h\vartheta \rightarrow 2HO^{\bullet} \quad (32)$$

$$TiO_2 + h\vartheta \rightarrow e_{CB}^{-} + h\vartheta_{VB}^{+} \quad (33)$$

$$h\vartheta_{VB}^{+} + HO^{-} \rightarrow HO^{\bullet} \quad (34)$$

$$h\vartheta_{VB}^{+} + H_2O \rightarrow HO^{\bullet} + H^+ \quad (35)$$

Sonolysis is another AOP technique that utilizes ultrasound radiation to generate HR through the process of water pyrolysis. In the sonolysis process, the acoustic cavity of bubbles plays a key role in HR generation. The formation, growth, and implosive collapse of bubbles could be controlled by changing the power and frequency (Eqs.(36)–(40)) [63].

$$H_2O \xrightarrow{)))} HO^{\bullet} + H^+ \quad (36)$$

$$HO^{\bullet} + HO^{\bullet} \rightarrow H_2O_2 \quad (37)$$

$$H_2O_2 + HO^{\bullet} \rightarrow HO_2^{\bullet} + H_2O \quad (38)$$

$$HO_2^{\bullet} + HO_2^{\bullet} \rightarrow H_2O_2 + O_2 \quad (39)$$

$$HO_2^{\bullet} + H_2O_2 \rightarrow HO^{\bullet} + H_2O + O_2 \quad (40)$$

Ozonation is the other approach for HR generation. The following equations are proposed for the HRs generation by O_3 (Eqs.(41)–(45)) [64].

$$O_3 + OH^- \rightarrow HO_2^- + O_2 \quad (41)$$

$$HO_2^- + O_3 \rightarrow O_2^{\bullet -} + HO_2^{\bullet -} \quad (42)$$

$$HO_2^{\bullet -} \rightarrow O_2^{\bullet -} + H^+ \quad (43)$$

$$O_3 + O_2^{\bullet -} \rightarrow O_3^{\bullet -} + O_2 \quad (44)$$

$$O_3 + H_2O \rightarrow HO^{\bullet} + O_2 + OH^- \quad (45)$$

in comparison with single metal oxides, Cu/Fe bimetal oxide has been shown high catalytic activity due to the synergism of Cu–Fe active sites. The Cu plays a significant role via donating the electron to ferric in order to reduce to ferrous. Meanwhile, the catalytic activity of $CuFeS_2$ is more than Cu/Fe bimetal because the S^{2-} is an electron donor resulting in enhancing the Fe^{3+}/Fe^{2+} cycle. Nie W et al. (2019) have compared the PMS activation for BPA removal by $CuFe_2O_4$ and $CuFeS_2$. The reported that bimetallic sulfide was much effective than bimetallic oxide due to effect of S^{2-} in improving of Fe^{3+}/Fe^{2+} and Cu^{2+}/Cu^{+} cycles (Fig. 3) [42].

5. Effect of the operational parameters on oxidant activation by $CuFeS_2$

Table 1 provides a summary of the effectiveness of advanced oxidation processes (AOPs) were initiated by chalcopyrite, with regards to its ability to oxidize of organic pollutants. The effect of different operational parameters including pH, catalyst dosage, and oxidant concentration is presented. Table 2 provides the removal efficiency of pollutants by Fe, Cu, and Cu–Fe-based catalysts for oxidants activation. As shown the removal efficiency for Fe and Cu oxidants activators is much less than Cu–Fe oxidants activators suggesting the synergic effect of Fe and Cu for oxidants activation and ROS generation. Although experimental conditions such as pH, oxidant concentration, catalyst dosage, etc. Have an effect on the oxidation process, the comparison of pollutant removal efficiencies using chalcopyrite with other copper and iron based catalysts showed that $CuFeS_2$ has suitable efficiencies.

5.1. Effect of pH on catalytic activity of $CuFeS_2$

pH is the most important parameter in chemical reaction. The effect of pH was studied in the presence of different systems. The results demonstrated that in the $CuFeS_2$/PMS system, pollutant degradation exhibited greater efficacy in acidic conditions compared to natural and alkaline conditions. This can be attributed to the fact that the activation of PMS by $CuFeS_2$ in an acidic environment leads to the generation of a higher quantity of sulfate radicals. Moreover, with increasing pH,the $SO_4^{\bullet -}$ tend to undergo conversion to the $^{\bullet}OH$. Therefore, the low redox potentials and half-life time of $^{\bullet}OH$ compared to $SO_4^{\bullet -}$ radicals contribute to a reduction in the overall removal efficiency [92,93].

The study of Li Y et al. (2021) showed the removal efficiency in $CuFeS_2$/percarbonate (PC) system has proper efficiency in the wide

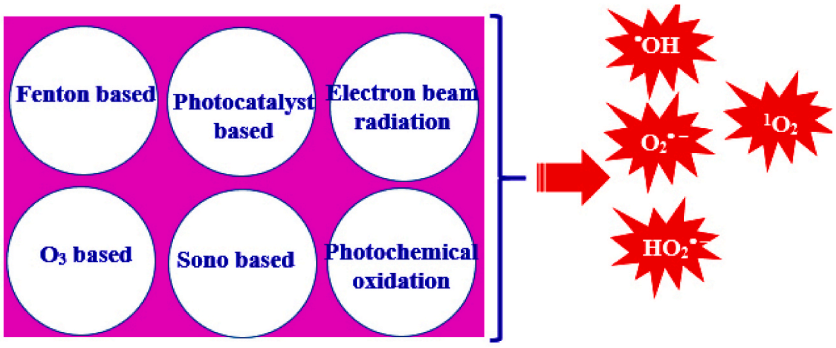

Fig. 3. Approaches used for HR generation.

Table 1
Degradation efficiency of chalcopyrite/oxidants systems.

Pollutant	Pollutant concentration (mg/L)	pH	Oxidant Concentration (mM)	molar ratio of oxidant/pollutant	Chalcopyrite dosage (g/L)	Reaction time (min)	Reactive species	Solution matrix	Light source	Pollutant removal (%)	Ref.
2,4-dichlorophenol (2,4-DCP)	10	7	60 (H_2O_2) & 25 (PC)	978 and 407	0.5	120	$^{\bullet}OH$, $^1O_2$, $^{\bullet}CO_3^-$ & $O_2^{\bullet -}$	DW	–	90	[37]
yellow tartrazine (YT) dye	75	3	0.25 (H_2O_2)	1.78	0.25	60	$^{\bullet}OH$ & $O_2^{\bullet -}$	Ethanol/DW	Red LED Green LED Blue LED White LED	88.1 81.4 67.7 64.3	[41]
Bisphenol A (BPA)	20	6	0.3 (PS)	3.5	0.1	20	$^{\bullet}OH$ & $SO_4^{\bullet -}$	Ultrapure Water	–	99.7	[42]
bisphenol A (BPA)	20	6	20 (H_2O_2)	228	0.2	60	$^{\bullet}OH$	DW	Fluorescent	97.4	[43]
Tartrazine	100	3	8.33 (H_2O_2)	44	0.2	150	$^{\bullet}OH$	DW	Fluorescent	99.1	[44]
Sulfamethazine	5	7.1	0.8 (PC)	44	0.5	40	$^{\bullet}OH$	Ultrapure Water	–	89.6	[65]
Bisphenol S (BPS)	2.5	11	0.4 (PS)	40	2	30	$O_2^{\bullet -}$	DW	–	80	[66]
Acid orange 7 (AO7)	100	6.26	40 (H_2O_2)	140	2	30	$^{\bullet}OH$	DW	–	100	[67]
Rhodamine B	10	5.2	39.2 (H_2O_2)	1877	6	120	$^{\bullet}OH$	surface water	–	96.5	[68]
Rhodamine B	20	4	0.4 (PS)	9.5	0.02(C–$CuFS_2$) 0.02 (H–$CuFS_2$)	20	$^{\bullet}OH$ & $SO_4^{\bullet -}$	Textile wastewater	–	70 96.84	[69]
Carbamazepine	5	6.76	5 (PS)	236	1	30	$SO_4^{\bullet -}$	DW	–	82.34	[70]

Table 2
Degradation efficiency of pollutants using Fe, Cu and Fe–Cu based catalysts.

Catalyst	pollutant	Pollutant concentration	Catalyst dosage	Oxidant/ concentration	Reaction time	Removal efficiency (%)	Ref
Cu^0/Fe^3O^4	4-chlorophenol	0.1 mM	1.0 g/L	H_2O_2/0.03 Mm	1 h	100	[71]
FeS_2	P-chloroaniline	0.62 mM	4.0 g/L	H_2O_2/0.03 Mm	6 h	55	[72]
FeS_2	Trichloroethylene	0.268 mM	100 g/L	H_2O_2/0.05 Mm	323 h	98	[73]
FeS_2	Diclofenac	25 mg/L	0.12 g/L	H_2O_2/0.03 Mm	0.33 min	100	[74]
Surface-oxidized FeS_2	Arsenite (Sb(III))	20 μM	0.25 g/L	H_2O_2/0.03 Mm	2 h	100	[75]
Fe^{2+}	Chlorobenzene	1 mM	2 mM	PC/2.0 mM	1 h	94.06	[76]
Fe^{2+}	Benzene	1 mM	10 mM	PC/10 mM	0.17 h	99.99	[77]
Fe^{2+}	Sulfamethoxazole	0.06 mM	0.5 mM	PC/0.6 mM	1 h	94.1	[78]
Fe^{2+}	Acetaminophen	0.05 mM	1.0 mM	PS/0.8 Mm	0.5 h	81.4	[79]
Fe^{2+}	Sulfadiazine	100 μM	1.0 mM	PS/4 mM	2 h	100	[80]
Fe^{2+}	Trimethoprim	1 mM	4.0 mM	PS/4 mM	4 h	73	[81]
Fe^{2+}	Chlortetracycline	1 mM	1000 mM	PS/500 mM	2 h	76	[82]
Cu^{2+}	Benzophenone-3	1.31 μM	0.5 mM	PDS/131 μM	11 h	39	[83]
Cu^{2+}	p-nitrophenol	0.72 mM	30 mM	PDS/30 mM	3 h	14	[84]
Cu^{2+}	Bisphenol A	10 μM	15 μM	PMS/1.0 mM	0.25 h	16	[85]
Cu^{2+}	Naproxen	5 μM	10 μM	PMS/0.5 mM	0.08 h	6.9	[86]
$CuFeO_2$	Orange I	4 mg/L	0.1 g/L	PMS/20 μM	0.5 h	77.8–79.3	[87]
$CuFe_2O_4$	Norfloxacin	25 μM	0.2 g/L	PMS/0.5 mM	2 h	90	[88]
$CuFe_2O_4$	*p*-nitrophenol	50 mg/L	30 g/L	PDS/8 mM	1 h	89	[89]
$CuFe_2O_4$	Tetrabromobisphenol A	10 mg/L	0.1 g/L	PMS/0.2 mM	0.5 h	99	[90]
$CuFe_2O_4$	Atrazine	2.0 μM	0.1 g/L	PMS/1.0 mM	0.25 h	98	[91]

range pH. However, the highest removal was obtained for acidic conditions, but the leaching of metal is high causing secondary pollution and restricting the $CuFeS_2$/PC application. While the pollutant degradation was proper in neutral pH with minimum metal leaching. In this work, the low efficiency has been attributed to the negative charge of $CuFeS_2$ and the anionic form of pollutant in the alkali pH that hindered the pollutant adsorption by the catalyst due to electrostatic repulsion. Moreover, at alkali pH, the self-decomposition of H_2O_2 to water and oxygen causes less ROS generation. As well as the precipitation of metal ions increases leading to a reduction of the synergistic effect between Fe (II) and Cu (I) resulting in low accessibility of catalytic sites [65]. The study of Peng J et al. (2020) have reported the highest removal efficiency of BPS in $CuFeS_2$/PMS system was obtained under acidic condition, however, PMS alone was more activated under alkali condition and BPS degradation (57.8%). Moreover, although the leaching of Cu and Fe is high in the acidic pH, the activation rate of PM is very low in acidic conditions because metals arrive in the hydroxide form, and cannot be effective in PMS oxidation. They have concluded the low DBP degradation in alkali pH is related to the pK_a of PMS and the pH_{zpc} of the catalyst. Since the PMS charge at different pH is negative (pK_{a1} and pK_{a2} of PMS = 0 and 9.4 respectively), while the pH_{zpc} of the catalyst is 4, thus, the surface charge of the catalyst will be positive at pH < 4 and negative at pH > 4. Therefore, PMS activation by the catalyst will be decreased at pH > 4 due to the repulsion force (Fig. 4a) [66].

5.2. *Effect of catalyst dosage*

Catalyst dosage is the key parameter in the degradation process. Different studies have shown the degradation rate of pollutants is enhanced by increasing of the catalyst dosage (Fig. 4b). The study of Wu Y et al. (2023) showed the degradation efficiency was increased from 35.14% to 70.63% with increasing of natural chalcopyrite dosage from 2.5 mg/g_{soil} to 7.5 mg/g_{soil}. They concluded the high dosage of catalyst provide more active sites for activation of PMS/H_2O_2, result in more ROS generation. Nonetheless, further catalyst dosage induces low ROS generation due to scavenging effect [94]. Moreover, the efficiency of pollutant removal may decline

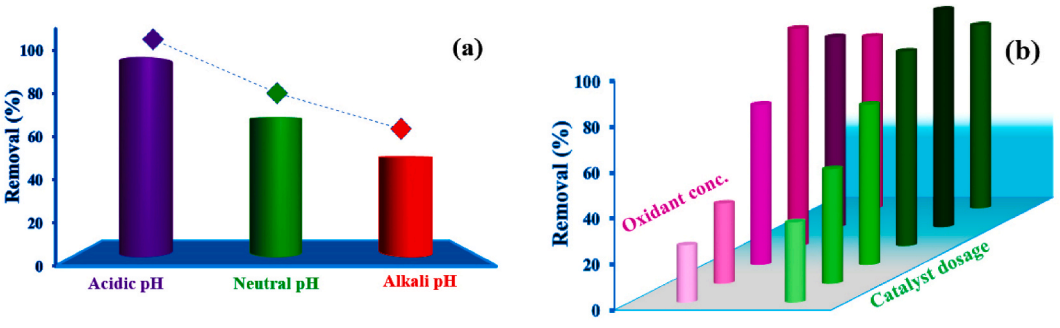

Fig. 4. a) effect of pH on $CuFeS_2$ based AOPs b) effect of oxidant concentration and catalyst dosage on $CuFeS_2$ based AOPs.

after reaching the optimum catalyst dosage, as a result of delayed mass transfer and restricted access to active sites at high catalyst dosage. This can occur due to the formation of diffusion boundary layers, inactive catalyst surfaces, and limited diffusion resulting from the aggregation of catalyst particles, which ultimately leads to reduced catalytic activity and efficiency [95–97].

Barhoumi et al. (2017) evaluate the effect of chalcopyrite dosage in the photo-Fenton process. Results revealed the removal efficiency of pollutants was increased with increasing of catalyst dosage up to 1.0 mg/L. The further dosage had no significant effect on removal efficiency due to more ferrous ions release and their reaction with $^{\bullet}OH$ radicals [30]. The study of Wu Y et al. (2023) confirmed that extra catalyst dosage leads to the deadweight loss of ROS [94]. Li Y et al. (2021) have reported a similar result. This work showed the removal efficiency increased with the raising of the catalyst dosage up to 0.5 g/L (86.4%). While excessive catalyst dosage leads to the deadweight loss of active radicals and environmental risk due to high metals leaching into the solution [65]. Peng J et al. (2020) investigated the effect of the catalyst dosage. The results of this work revealed with increasing the catalyst dosage from 0.2 g/L to 2 g/L, the removal efficiency was increased by 32.2%, while the removal efficiency was increased by 0.4% for 3 g/L of $CuFeS_2$ dosage. This work suggested that the radical production process in different catalyst dosages is related to the oxidant concentration. Therefore, the catalyst dosage should be proportional to the oxidant concentration to enable its activation. They concluded active sites on $CuFeS_2$ at 2 g/L is adequate for 0.4 mM PMS activation and further catalyst dosage do not participate in degradation process [66].

5.3. Effect of oxidants concentration

Oxidants are the source of ROS; therefore play the significant role in the pollutant degradation process. Study of Wu Y et al. (2023) indicated with increasing of PMS/H_2O_2 from 2.5 mg/g_{soil} to 12.5 mg/g_{soil}, the removal efficiency was 25% increased. This due to accelerating of ROS generation in optimum concentration of the oxidants [94]. Li Y et al. (2021) have reported the further concentration of the H_2O_2 caused the decrease in the removal efficiency due to the scavenging effect of H_2O_2 and generation of the weak ROS ($^{\bullet}OOH$) (Eqs. (46) and (47)). Moreover, excessive concentration of H_2O_2 leads to an increase in solution alkalinity which is the improper condition for Fenton-based reactions [65]. Peng J et al. (2020) have reported the removal efficiency of bisphenol S was increased by 43% with increasing the PMS concentration from 0.1 to 0.6 mM. They reported more ROS is generated at high PMS concentrations (up to 0.6 mM) and further PMS concentrations do not change the removal efficiency due to reaction between sulfate radicals which each other (Eqs. (48) and (49)) (Fig. 4b) [66].

$$H_2O_2 + HO^{\bullet} \rightarrow H_2O + HOO^{\bullet} \quad (46)$$

$$HOO^{\bullet} + HO^{\bullet} \rightarrow H_2O + O_2 \quad (47)$$

$$SO_4^{\bullet -} + SO_4^{\bullet -} \rightarrow S_2O_8^{2-} \quad (48)$$

$$SO_4^{\bullet -} + HSO_5^{-} \rightarrow SO_5^{\bullet -} + SO_4^{2-} + H^+ \quad (49)$$

6. Chalcopyrite in fenton, photo-fenton and photo/fenton-like approach

Fenton is one of the most used AOPs methods regarding organic pollutants removal. Fenton's method is based on the electron transfer between hydrogen peroxide and Fe^{2+}/Fe^{3+} as a catalyst [98]. This approach is the most cost-effective AOPs due to the no energy required. The H_2O_2 activation by materials containing iron leads to hydroxyl radical generation. The degradation process could occur via hydroxyl radicals attacking the target organic pollutant. The following equations are suggested in the classical Fenton reaction (Eqs. ((7), (38), (39), (50)–(53)) [99].

$$Fe^{3+} + H_2O_2 \rightarrow Fe^{2+} + HO_2^{\bullet} + H^+ \quad (50)$$

$$HO^{\bullet} + Fe^{2+} \rightarrow Fe^{3+} + HO^- \quad (51)$$

$$Fe^{3+} + HO_2^{\bullet} \rightarrow Fe^{2+} + O_2H^+ \quad (52)$$

$$Fe^{2+} + HO_2^{\bullet} + H^+ \rightarrow Fe^{3+} + H_2O_2 \quad (53)$$

Photo-Fenton is one of the modified forms of traditional Fenton that is a combination of light radiation with Fenton [100]. The studies have suggested the recovery of the Fe^{2+} in the Fenton process is slow. Light irradiation is the proper alternative for accelerate the Fenton process and ferrous regeneration. $[Fe(OH)]^{2+}$ is the key photoactive iron complex in photo-Fenton process. $[Fe(OH)]^{2+}$ is reduced to Fe^{2+} under light irradiation (Eq. (11)) [101].

Fenton-like is the process which used the hetero-/homogeneous catalyst instead of Fe^{2+} for activation of oxidants [102]. The ferric ions, pyrite, copper, nZVI and etc. are the most popular materials that used in Fenton-like process. One of the prominent features of chalcopyrite catalyst is the possibility of performing both Fenton and Fenton-like reactions due to the release of Fe^{2+} and Cu^{+} decomposition of H_2O_2 to form ROS (Eqs.1,7- 9) [36,68].

Ltaïef AH et al. (2018) used the mined chalcopyrite as catalysts for the oxidation of phenolic pollutants using Fenton and LED photo-Fenton-like. Results showed 98% of mineralization was achieved. This study suggested rapid leaching of iron species (ferrous &

Table 3
Degradation efficiency of Electrochemical Fenton-based processes using chalcopyrite.

pollutant	Pollutant concentration (mg/L)	Anode	Cathode	Electrode distance (cm)	Electrolyte/ Concentration	Current intensity (mA cm^{-2})	Chalcopyrite (g/L)	H_2O_2 source	Reactive species	Light source	Pollutant removal (%)	Ref.
Acid orange 7	98	boron-doped diamond (BDD)/ Si	carbon felt	1.0	Na_2SO_4/0.05 M	300	2.0	Electro generated	•OH	UVA	95	[36]
Cephalexin	50	IrO_2/air-diffusion cell	–	1.0	Na_2SO_4/0.05 M	50	1.0	Electro generated	•OH	UVA	100	[40]
Tetracycline	89	Pt mesh/thin-film BDD onto a Nb	3D carbon felt	–	Na_2SO_4/0.05 M	500	1.0	Electro generated	•OH	–	98	[40]

ferric) in the presence of O_2 which leads to H_2O_2 generation without being added due to the reaction of ferrous ions and oxygen molecules via the Haber–Weiss reaction (Eq. (3), (54)–(56)).

$$Fe^{2+} + 4O_2 \rightarrow Fe^{3+} + O_2^{\bullet -} \tag{54}$$

$$Fe^{2+} + O_2^{\bullet -} + 2H_2O \rightarrow Fe^{3+} + 2OH^- + H_2O_2 \tag{55}$$

$$Fe^{2+} + O_2^{\bullet -} + 2H^+ \rightarrow Fe^{3+} + H_2O_2 \tag{56}$$

in the photo-Fenton-like process, the chalcopyrite showed high photocatalytic activity due to copper content which has high absorption spectrum at the LED irradiation [39].

Huang X et al. (2020) evaluated the effect of p- and n-type chalcopyrite in the Fenton oxidation process. Results showed n-type chalcopyrite has high catalytic activity because it releases more Cu^+ and Fe^{2+} ions and less Cu^{2+} release that leads to more H_2O_2 activation. Because Cu^+ and Fe^{2+} ions can easily donate one electron to H_2O_2 and improve its decomposition for more ROS generation. Moreover, the pH is further decreased for the n-type catalyst compared to the p-type which provides a better condition for the Fenton process. Results indicated the removal efficiency of acid orange 7 was obtained 60% and 100% at a natural pH for p- and n-type chalcopyrite/H_2O_2 system respectively [67]. The da Silveira Salla J et al. (2020) have reported that $Fe^{2+/3+}$ and $Cu^{1+/2+}$ present on the catalyst surface are responsible for H_2O_2 decomposition and $^{\bullet}OH/O_2^{\bullet -}$ generation [44].

7. Electrochemical Fenton-based processes using chalcopyrite

Electrochemical oxidation (EO) is one branch of the AOPs used for the degradation of refractory organic pollutants. EO is considered an eco-friendly approach in order to generate a high amount of reactive radicals [103,104]. Table 3 presented the degradation efficiency of Electrochemical Fenton-based processes using chalcopyrite. This table provides the summary of parameters ranges which used in EO process in the presence of chalcopyrite. The main advantages of the Electro-Fenton process compared to Fenton methods include: 1) in-situ H_2O_2 production and prevention of risks related to its transportation, storage and management 2) The possibility of controlling the decomposition kinetics and 3) Higher decomposition rate of pollutants due to regeneration of Fe^{2+} in the cathode and also minimization of sludge production [105]. According to Fenton's reagent addition or radical formation, the Electro-Fenton process is classified into 4 categories: 1) H_2O_2 and Fe^{2+} are electro-generated using a sacrificial anode and an oxygen sparging cathode respectively 2) Fe^{2+} is generated from the sacrificial anode and H_2O_2 externally added 3) Fe^{2+} is externally added and H_2O_2 generated by oxygen sparging cathode 4) $^{\bullet}OH$ is generated by Fenton reagent in an electrolytic cell and Fe^{2+} regenerated due reduction of Fe^{3+} on the cathode [106].

In the study conducted by Droguett C et al. (2020), it was observed that the concentration of electrogenerated H_2O_2 increased with higher current density. However, upon adding chalcopyrite to the system, the H_2O_2 concentration decreased from 44.0 mM to 4.5 mM, leading to the generation of ROS. The result indicated copper ions enhanced the Fe^{2+} regeneration. Moreover, UVA irradiation showed a positive effect on cephalexin removal. However, the role of adsorption (2.2%) and photolysis alone (3%) were low in antibiotic removal, while the chalcopyrite/UVA system showed remarkable efficiency in removal (36%). In the photoelectro-Fenton system, current density and catalyst concentration are the main keys in the removal process. Result indicated the increasing of the current density up to 100 mA cm^{-2} leads to yielding more $^{\bullet}OH$. Further current density causes side reactions that destroy the IrO_2 and decrease the removal efficiency. As well as, increasing the chalcopyrite dosage up to 1 g/L increased the removal efficiency by more generation of oxidant $^{\bullet}OH$ from Fenton's reaction. While the removal efficiency decreased with increasing the catalyst dosage >1.0 g/L due to the reaction of $^{\bullet}OH$ with an excess of dissolved Fe^{2+} (Eq. (47)) [40].

Labiadh L et al. (2019) used boron-doped diamond (BDD)/Si and carbon felt as anode and cathode respectively. The result indicated the TOC removal increased in the presence of chalcopyrite (up to 2.0 mg/L) due to more release of Fe^{2+} and Cu^{2+} from the catalyst surface which enhanced the $^{\bullet}OH$ generation. This study revealed that H_2O_2 can be electrogenerated under O_2 saturation. Then the hydrogen peroxide contributes to ROS generation and Cu^+ and Fe^{2+} regeneration (Eqs.(57)–(59)).

$$Cu^{2+} + H_2O_2 \rightarrow Cu^+ + HO_2^{\bullet} + H^+ \tag{57}$$

$$Cu^+ + HO_2^{\bullet} \rightarrow Cu^{2+} + H^+ + O_2 \tag{58}$$

$$Cu^{2+} + R^{\bullet} \rightarrow Cu^+ + R^+ \tag{59}$$

Moreover, the Cu^{2+}/Cu^+ couple participates in ROS generation, Fe^{2+} regeneration and improves the catalytic activity by prolonging the Fe^{3+}/Fe^{2+} cycle (Eq. (60)).

$$Cu^+ + Fe^{3+} \rightarrow Cu^{2+} + Fe^{2+} \tag{60}$$

The findings also demonstrated that an increase in current density resulted in a higher rate of degradation of contaminants. This can be attributed to the greater generation of H_2O_2. Furthermore, BDD electrode plays the key role in $^{\bullet}OH$ generation. Because BDD electrode has great oxidation power, high oxygen evaluation and lower physisorption of hydroxyl radical which makes $^{\bullet}OH$ available for pollutant degradation [36].

The study of Barhoumi N et al. (2017) has also confirmed both Fenton (Fe^{2+}/H_2O_2) and Fenton-like (Cu^{2+}/H_2O_2) processes

contribute to pollutant degradation in the electro-Fenton (EF)/$CuFeS_2$ process. Moreover, Cu^{2+} is reduced at the cathode and induces the regeneration of Fe^{2+} by Cu^{+} (Eqs. (60) and (61)).

$$Cu^{2+} + e^{-} \rightarrow Cu^{+} \quad (61)$$

Results indicated increasing of the $CuFeS_2$ dosage leads to more Fe^{2+} and Cu^{2+} generation (limiting step) and high $^{\bullet}OH$ formation. Furthermore, findings revealed the EF-BDD/Chalcopyrite process is more effective than EF- Pt/Chalcopyrite process in pollutant removal. This has been attributed to the high oxygen evaluation by BDD compared to the Pt electrode. The mineralization of the tetracycline (TC) showed the NH_4^+ and NO_3^- ions are detected which confirmed the TC degradation with the difference that more NH_4^+ concentration is accumulated in EF/Chalcopyrite with BDD anode compared to the EF/Chalcopyrite with Pt anode due to more TC degradation [30].

8. Proposed catalytic mechanism

Depending on the type of reaction (PS, Fenton, photo-Fenton, electro – Fenton and etc.), different mechanisms have been proposed in pollutant removal by $CuFeS_2$ activation of oxidants (Fig. 5 a-d). Huang X et al. (2020) have reported the mechanism of pollutant degradation in Fenton oxidation by natural pyrite occurs in two consecutive stages. First, the chalcopyrite metals content, including Cu^{+}, Cu^{2+}, and Fe^{2+} ions are released into the solution. Second, the released ions react with H_2O_2, generating ROS and inducing AO7 degradation. This study also verified that the excessive release of Cu^{2+} hampers the removal of AO7 due to the formation of intermediate products in the form of Azo metal complexes (Fig. 5a) [80].

In the photo – Fenton process, electron–hole pairs are generated under light irradiation. The Chang SA et al. (2020) used the PL analysis to evaluate the quantify recombination rate of the electron–hole pairs. This work showed the weak intensity luminescence emission for $CuFeS_2$ due to the lowest yield of electron–hole pairs (Fig. 5b) [45]. In the photocatalyst approach, ROS generation is the main mechanism for pollutant degradation and active sites on the catalyst can play the main role in this regard [9]. Therefore, different scavengers have been employed for the determination of the involved ROS in the photocatalyst process. Vieira Y et al. (2022) used the IPA, BQ, and EDTA scavengers to evaluate the role of $^{\bullet}OH$, $^{\bullet}O_2^-$ and h^+ radicals in the $CuFeS_2/H_2O_2$/red and white light system. The results indicated that under both red and white light irradiation, the ROS involved are predominantly $^{\bullet}OH$, whereas $^{\bullet}O_2^-$ plays a minor role in the degradation process. Results also confirmed that h^+ has not been involved in pollutant degradation [41]. In order to assess the degradation of Rhodamine B (RhB) in the Fenton process, Yang J et al. (2022) utilized TBA and IPA to quench the $^{\bullet}OH$ radicals present on the catalyst surface and in solution, respectively. Results showed the removal efficiency of RhB degradation was decreased

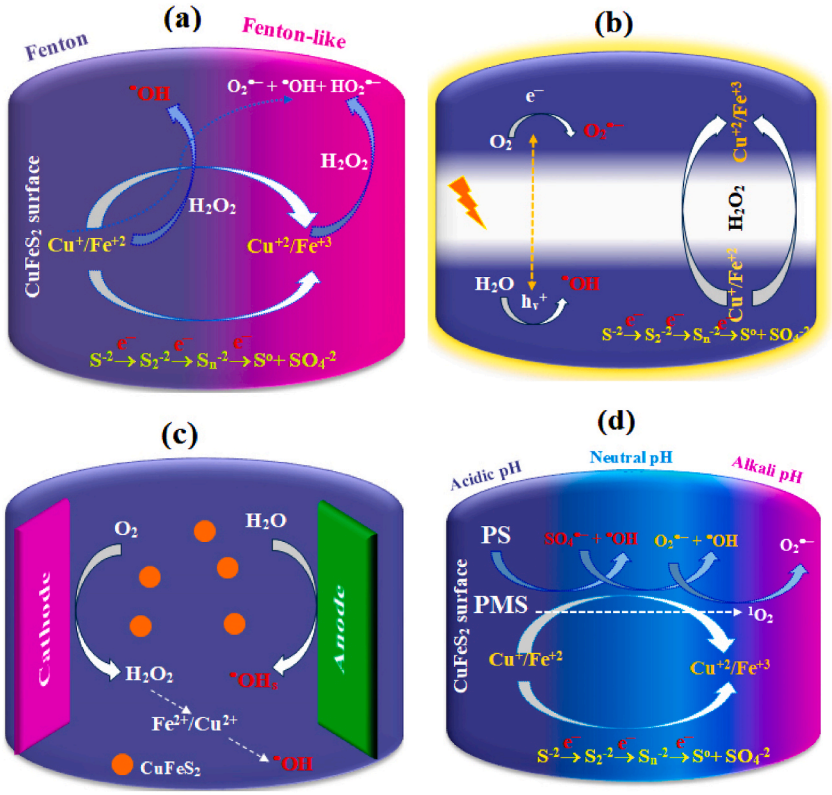

Fig. 5. The mechanism of ROS generation in different approaches.

in the presence of IPA compared to the TBA suggesting the $^{\bullet}OH$ in solution has dominant role in degradation process. They used the DMPO-trapped EPR spectrum to identify the ROS. The results indicated that the generation of $^{\bullet}OH$ radicals occurred exclusively in the presence of chalcopyrite, suggesting the activation of H_2O_2 by the Cu and Fe sites of the catalyst. In this work, the calcein and 2, 2′-dipyridyl were used to determine the role of the Fe^{3+} and Fe^{2+} respectively in H_2O_2 decomposition. Results showed that leached iron played a minor role in H_2O_2 activation and consequently in pollutant degradation. While leached copper played remarkable role ROS generation. However, the reaction between Fe^{3+} and Cu^{+} in $CuFeS_2$ causes the improvement of the Fe^{2+}/Fe^{3+} and Cu^{+}/Cu^{2+} cycles. Besides, the sulfur through reducing Cu^{2+} and Fe^{3+} enhances the catalytic activity of $CuFeS_2$ [68].

Da Silveira Salla J et al. (2020) proposed three scenarios involved in pollutant degradation in microwave–assisted photo–Fenton oxidation: a) The Fe^{2+}/Fe^{3+} complex present on the surface of the catalyst induces H_2O_2 decomposition, $^{\bullet}OH$ generation due reaction of Fe^{2+} and H_2O_2 and reduced Fe^{3+} to produce the Fe^{2+} which reacts again with H_2O_2 b) Cu^{+} and Cu^{2+} react with H_2O_2, generates the $^{\bullet}OH$ c) using of chelating agent in the catalyst synthesis process causes a decrease in the redox potential of the Fe^{2+}/Fe^{3+} complex, improving the oxidation/reduction reactions [44].

Droguett C et al. reported the mechanism of the electro-Fenton (EF) method. In this approach, two mechanisms are involved in pollutant degradation: first, iron and copper ions released from the electrode create the homogeneous catalysis. These ions activate the H_2O_2 and generate the $^{\bullet}OH$ radicals. Simultaneously, the $^{\bullet}OH$ radicals are generated at the anode surface. Moreover, the different mechanisms include a) pollutant adsorption on chalcopyrite powder, b) photolysis (irradiation of light), and c) chalcopyrite/light photocatalysis in the photo-electro-Fenton process.

This study indicated that in the electro-Fenton process, the involvement of the •OH radical in the degradation of organic pollutants is diminished due to its reaction with by-products, such as short-chain carboxylic acids. Consequently, this reaction leads to a decrease in the removal efficiency. In contrast, in the photoelectron-Fenton process the UV photons could photodegrade the carboxylic acid-s−Fe^{3+} complex and generate the ROS (Eq. (62)) [40].

$$Fe\ (OOCR)^{2+} + h\vartheta \rightarrow Fe^{2+} + CO_2 + R^{\bullet} \tag{62}$$

Labiadh L et al. (2019) explained the degradation mechanism of AO7 in the EF process with chalcopyrite as an iron source. Results showed the synergic effect between Fe/Cu ions that improve the EF system. The generated Cu^{2+} react with $HO_2^{\bullet}$ or/and $R^{\bullet}$ is reduced to Cu^{+}. Afterward, carbon felt (cathode) regenerate the Fe^{2+} and Cu^{2+} which facilitate the Fenton reaction to produce the $^{\bullet}OH$. The $Fe^{2+/3+}$ cycles can be prolonged due to regeneration of Fe^{2+} by the Cu^{+}/Cu^{2+} couple. Moreover, in the EF process, the H_2O_2 can be produced which enhances the formation of hydroxyl radicals from the Fenton reaction. On the other hand, the BDD ($^{\bullet}OH$) is generated in the anode side via a reaction with the water molecules. Therefore, pollutants are adsorbed by the anode surface due to the "physisorbed" phenomenon and be oxidized by BDD ($^{\bullet}OH$) (Fig. 5c) [36].

Wu Y et al. (2023) evaluate the ROS involved in the $CuFeS_2/PMS/H_2O_2$ system. This work showed the mechanism of pollutant degradation is included a) contribution of surface Cu^{+} and Fe^{2+} in PMS/H_2O_2 activation, which generate the $SO_4^{\bullet-}$ and $^{\bullet}OH$ radicals b) $O_2^{\bullet-}$ can be generated through various mechanisms, including the reaction of PMS with H_2O molecules, activation of oxygen molecule via single electron transfer of the $CuFeS_2$, and the reaction of Fe^{2+} with oxygen molecules c) reductive sulfur species such as S^{2-} and S_n^{2-} react with surface Cu^{2+} and Fe^{3+}, thereby reducingthem to Cu^{+} and Fe^{2+}. This reduction process contributes to the continuous formation of active radicals d) the reaction of Fe^{3+} with $O_2^{\bullet-}$ and electron transfer, facilitate the regeneration Fe^{2+} which contribute to activation of the PMS/H_2O_2 [94].

Li Y et al. (2021) have reported that O_2 can be reduced to $O_2^{\bullet-}$ by surface Fe^{2+} and Cu^{+} of $CuFeS_2$ catalyst via single-electron transfer route. Moreover, the standard redox potential vs. RHE for $O_2/O_2^{\bullet-}$, Fe^{3+}/Fe^{2+} and Cu^{2+}/Cu^{+} is −0.33, 0.77 and 0.17 respectively which suggested proper thermodynamically condition for regeneration of Fe^{2+} and Cu^{+} (Eqs. (63) and (64)) [65].

$$Fe^{3+} + O_2^{\bullet-} \rightarrow Fe^{2+} + O_2 \tag{63}$$

$$Cu^{2+} + O_2^{\bullet-} \rightarrow Cu^{+} + O_2 \tag{64}$$

Wen PY et al. (2022) used the methanol and NaN_3 as $^{\bullet}OH$ and $SO_4^{\bullet-}$ scavengers to evaluate the degradation mechanism of RhB in the $CuFeS_2/Na_2S_2O_8$ system. Results indicated the Fe^{2+}/Cu^{+} on the $CuFeS_2$ surface catalyzed persulfate to $SO_4^{\bullet-}$ radicals. Subsequently, the $SO_4^{\bullet-}$ reacts with H_2O/OH^{-} to generate the $^{\bullet}OH$ radicals. The quenching test illustrated adding the methanol into the reaction causes a slightly decreased in removal efficiency suggesting that $SO_4^{\bullet-}$ plays the dominant role in the degradation process. Also, the S^{2-} anions as reduction agents present in catalysts facilitate the Fe^{2+} regeneration [29]. Nie W et al. (2019) also reported a similar mechanism for the activation of peroxymonosulfate by $CuFeS_2$. This work confirmed the role of Fe^{2+} and Cu^{+} in ROS generation. Moreover, results showed S^{2-} and S_2^{2-} as strong reductive sulfur species cause the reduction of Cu^{2+} and Fe^{3+} to Cu^{+} and Fe^{2+} forms. Also, Cu^{+} via electron transfer induces reducing of Fe^{3+} to Fe^{2+}. This study confirmed that the Fe^{3+}/Fe^{2+} cycle on the chalcopyrite surface plays a significantly more substantial role compared to the Cu^{2+}/Cu^{+} cycle in oxidant activation. These findings suggest that Fe is a more crucial element in the $CuFeS_2$ catalyst [42]. The study of Peng J. (2020) illustrated that pH plays a remarkable role in the Fe^{3+}/Fe^{2+} and Cu^{2+}/Cu^{+} cycles. The result showed highest homogeneous catalytic activity of Fe^{3+} and Cu^{2+} ions occurred at pH = 6.2. Also, results suggested adding 50 μM of Fe^{3+} and Cu^{2+} enhances the pollutant degradation in the chalcopyrite/PMS system due to the regeneration of Fe^{2+} and Cu^{+} by S^{2-}. Moreover, Cu^{+} boosted the Fe^{3+}/Fe^{2+} cycling [66].

Li Y et al. (2021) reported the Cu^{+} and Fe^{2+} present in the catalyst surface have a key role in the percarbonate activation by chalcopyrite. As a result of percarbonate activation, the $^{\bullet}OH$ is produced which could be convert to other ROS including $CO_3^{\bullet-}$, $O_2^{\bullet-}$ and $^1O_2$. Moreover, the catalyst activates the O_2 molecules, generating the $O_2^{\bullet-}$. The produced $O_2^{\bullet-}$ together with S^{2-} species as well as the

interaction between Cu^{+} and Fe^{3+} improve the Fe^{3+}/Fe^{2+} cycles on the catalyst surface [65]. Peng J et al. (2020) studied the bisphenol S (BPS) degradation in the natural chalcopyrite/PMS system. The results showed depended on the pH condition, different radicals participate in the degradation process. So that the $^{\bullet}OH$ and $SO_4^{\bullet-}$ are the main ROS at acid or weak acid conditions. While, $O_2^{\bullet-}$ and $^{\bullet}OH$ are responsible at weak alkaline conditions and $O_2^{\bullet-}$ alone plays the main role at strong alkali pH for the BPS degradation. In this work, a similar mechanism is presented to express the role of Fe^{2+}, Cu^{+}, reductive sulfur species, and regenerated Fe^{2+} and Cu^{+} for continuously activating PMS to generate ROS which has been discussed previously [66].

In order to evaluate the mechanism of 2,4-dichlorophenol degradation, Xu X et al. (2019) employed the TBA, NaN_3 and BQ as radical scavengers for $^{\bullet}OH$, $^1O_2$ and $O_2^{\bullet-}$ respectively, in the peroxymonocarbonate/chalcopyrite system. The result showed the $^1O_2$ radical is a highly reactive ROS that significantly contributes to pollutant degradation. On the other hand, the quenching experiments indicated $O_2\bullet-$ does not play a role in the degradation process due to its very short half-life and sensitivity to protons. However, $O_2^{\bullet-}$ does play a role as an intermediary in the generation of $^1O_2$. This occurs when $^{\bullet}CO_3^{-}$ reacts with H_2O_2, resulting in the formation of bicarbonate and $O_2^{\bullet-}$ Subsequently, $O_2^{\bullet-}$ reacts with $^{\bullet}OH$, leading to the generation of $^1O_2$. This study showed the existence of HCO_3^{-} in the H_2O_2 solution induces modifying the ROS generation, and enriching the reactive species in the pollutant degradation process (Fig. 5d) [37].

9. Catalyst reusability and stability

Catalyst stability is the main parameter in the AOPs for long–term usage of catalysts and important parameter for the development of practical. Different approaches have been used to evaluate the reusability and stability of catalysts. Ltaïef AH et al. (2018) used three consecutive photo-Fenton like experiments. In this work $CuFeS_2$ catalyst was rinsed with water and dried in the oven at 70 °C for 6 h before each cycle. Three parameters including TOC conversion, H_2O_2 conversion, and leaching of Fe species during 1 h were evaluated. The result revealed that the TOC and H_2O_2 conversion were obtained at 98% and 87.5% in 1st cycle and decreased by 5.5% and 7.4% in 3rd cycle respectively. The leaching of the Fe was reported around 2 mg/L in three cycles. This work confirmed the proper stability of chalcopyrite (natural type) in a Fenton-like process due to high TOC removal in three consecutive cycles [39]. Da Silveira Salla J et al. (2020) used the 4 consecutive cycles for the evaluation of chalcopyrite (synthetic type) stability in the photo-Fenton process. Results showed that pollutant degradation and TOC removal were obtained at 97.4% and 82.3% in 1st cycle and decreased by 3.2% and 5.7% for the fourth cycle respectively. The Fe and Cu leaching were reported at 0.18 mg/L and 0.3 mg/L respectively which are less than 0.5% of the total metal content in the chalcopyrite. This issue suggested great stability and proper reusability of the catalyst in 4 consecutive cycles [43]. Vieira Y et al. (2022) evaluated the recyclability of chalcopyrite (synthetic type) in the photocatalytic process. Results showed the degradation rate was reduced 43.1% in fifth cycle compared to the 1st cycle. The Fe leaching was reported 0.0135 mg/L and Cu was below the detection limits of the method. For further investigation, the catalyst stability was evaluated by XRD analysis. The results revealed weak decreasing crystalline phase peak intensity occurred after 5 cyclic runs. This work suggested 3 factors involved in the decreasing of the catalytic activity of chalcopyrite after 5 reuses. a) reduction of Fe and Cu content due to leaching b) occupancy of the active site by degradation by-products c) the structural change resulting from improved radical species generation [41]. Chang SA et al. (2020) investigated the chalcopyrite (synthetic type) stability in the photocatalytic process. The result showed after 10 consecutive cycles, the pollutant degradation decreased from 97.5% to 15.0%. The XRD results revealed that the phase structure of the catalyst faded after 3 reaction runs. The SEM analysis confirmed the findings and showed an irregular sheet of catalyst changed to a spherical shape, suggesting improper stability of the catalyst. This work has proposed the incorporation of chalcopyrite with another catalyst (e.g. Ag_3PO_4) for improving the composite stability [45]. In another approach, Li Y et al. (2021) applied the XRD, SEM and EDS techniques for the evaluation of the chalcopyrite (synthetic type) stability. This study demonstrated that the oxidation process has an impact on the surface of the catalyst, resulting in the formation of new Cu and Fe (oxy)hydroxides. These (Oxy) hydroxides were appearing at $2\theta = 31.5^{\circ}$ and 39.9°. The SEM analysis confirmed the presence of rougher surface after reaction. Moreover, the EDS technique showed the existence of the C, O, and S elements due to the oxidation of the chalcopyrite oxidation, the deposition of the insoluble CO_3^{2-} and SO_4^{2-}. While the Cu and Fe signal was decreased after four consecutive reuses. However, the refreshing process of the catalyst using ultrasound in 0.1 M HCl resulted in an improvement in the removal efficiency. The removal efficiency, increased from 57.3% to 75.6%, indicating the positive effect of the refreshing process. The leaching test of metals showed low Cu and Fe release (<0.28 mg/L) which suggested the superior stability of the catalyst [65]. Peng J et al. (2020) also reported the removal efficiency was decreased by 21.6% due to change of chalcopyrite surface (synthetic type) during five consecutive cycles. The SEM analysis showed the catalyst surface is corroded and rougher after the oxidation process. Besides, the EDS technique illustrated the amount of Cu, Fe, and S decreased and the O element increased which suggested the changing structure of the catalyst after the reuse process. This work reported recovery of the catalyst by ultrasound (power: 70 W, frequency: 19.87 kHz, time reaction: 10 min) [66]. The study of Xi GY et al. (2022) investigate the chalcopyrite (natural type) stability in 4 consecutive cycles. Results showed the removal efficiency was decreased by 32.13%. They concluded the by-products generated during the oxidation process causes the deactivation of catalyst active sites [70].

Silveira Salla J et al. (2020) used the $CuFeS_2$ powders (synthetic type) in photo-Fenton process for 5 consecutive cycles. The results demonstrated a 5% decrease in removal efficiency and less than 1% Fe leaching after the fifth cycle. These findings strongly indicate that the implementation of a microwave-assisted procedure for catalyst preparation generally yields highly stable catalysts with remarkable reusability and sustained activity [44]. Nie Wet al. (2019) evaluate the stability of $CuFeS_2$ (synthetic type) in both controlled and uncontrolled pH. The Results showed that the leaching values of Cu and Fe are 3.8 mg/L and 1.8 mg/L, respectively. These values correspond to approximately 11% and 5.9% of the metal content present in the catalyst when the pH was not controlled. These findings illustrated the catalyst is unstable because the pH dropped from 6.0 to 3.6. When the pH was controlled at 6.0, the

leaching of Fe and Cu was reduced to 1.3 mg/L and 0.07 mg/L, respectively. Additionally, when using not PMS, the leaching of Fe and Cu decreased to 0.03 mg/L and 0.08 mg/L, respectively. These findings established that the acidic nature of the solution and oxidative dissolution have detrimental effects on the stability of the catalyst [42].

Droguett C et al. (2020) reused heterogeneous chalcopyrite (natural type) in Fenton-based electrochemical for 4 successive cycles. In this work ultrapure water and ethanol were applied for cleaning of the catalyst, drying under air in order to reuse. The result represented the long-term stability of the chalcopyrite. The metals leaching and pollutant degradation were not reported [40]. The reusability and stability of chalcopyrite (natural type) in electro-Fenton was conducted by Labiadh L et al. (2019). Results indicated the pollutant removal was decreased after some recycling due to deactivation of the active sites of the chalcopyrite because impurities content hinder the reaction between iron and oxidizer. The results of this work suggested the economic viability of catalyst due to 95% removal of TOC [36].

The stability evaluation showed the reusability of natural chalcopyrite is more the synthetic type (Fig. 6 a & b). Also, the recovery process has a direct impact on the activity of the catalyst. It was found that ultrasound-assisted recovery completely restores the catalytic ability of the catalyst. However, the recovery of the catalyst using ethanol and water fails to enhance the catalytic activity of chalcopyrite. Furthermore, the stability of the catalyst is also influenced by several factors, including pH control, the presence of oxidants, and the synthesis method employed, such as the utilization of microwave-assisted procedures.

10. Toxicity evaluation

Toxicity evaluation is a main parameter in the AOPs. The effluent of AOPs may induced the toxic materials result in ROS (e.g. ($^{\bullet}OH$, $SO_4^{\bullet-}$, $HO_2^{\bullet}$, $O_2^{\bullet-}$, $^{\bullet}CO_3^-$, $^1O_2$, O_3, e^- and etc.) reaction with pollutant target. Based on the physical and chemical characteristics, the intermediate products resulting from the degradation of raw materials may have a lower, equal or even higher level of toxicity than the main pollutants. Different toxicity approaches, including acute toxicity, genetic toxicity, estrogenic activity, immunity toxicity, and endocrine disrupting effect have been applied in order to evaluate the toxicity of the AOPs effluent [107].

Ltaïef AHet al (2018) used the two successive treatments (i.e. 1st and 3rd runs). utilizing Microtox® bioassays to evaluate the acute toxicity of the olive mill wastewater treated through chalcopyrite-based Fenton and LED photo-Fenton-like processes. Results indicated despite the high TOC removal (98.0 and 92.5% for 1st and 3rd runs, respectively), the inhibition of the luminescent activity of the bacteria was high due to toxicity effect of Fe^{2+} (25.9%) and Cu^{+} (84.8%). This work reported the toxicity caused by the catalyst was more than oxidation products. This finding raises significant concerns about the suitability and viability of using such catalysts, posing a serious challenge to their practical application. However, the Cu was more toxic than Fe (Fig. 7a) [39].

Vieira et al. (2020) employed a phytotoxicity approach to assess the toxicity of textile wastewater treated using rGO-$CuFeS_2$ catalyst in conjugated with microwave irradiation. Results showed the dye and TOC were decreased 97.7% and 99.11% respectively in 6 min reaction time. However, the toxicity was increased after 35 min due to formation of new toxic compounds caused by recombine of some nontoxic fragments (Fig. 7b) [69]. The study of Li Y et al. (2021) have reported the toxicity of sulfamethazine was decreased (bioaccumulation increased) except for P2 (4-nitrophenol/2- amino-4,6-dimethylpyrimidin-5-ol) and P6 (N-ethyl--N-methyl-N-(4-nitrophenyl) methanetriamine) in $CuFeS_2$/SPC process. This work suggested degradation process should be prolonged to reach the mineralization [65].

11. Challenges and future perspectives

The review highlights that although chalcopyrite has demonstrated promising results in advanced oxidation processes, there are still some challenges that need to be addressed.

1. Operational parameters including pH, temperature, oxidant concentration, and catalyst dosage have a significant effect on the efficiency of chalcopyrite-based oxidation processes. Therefore, further optimization of these conditions by experiment design

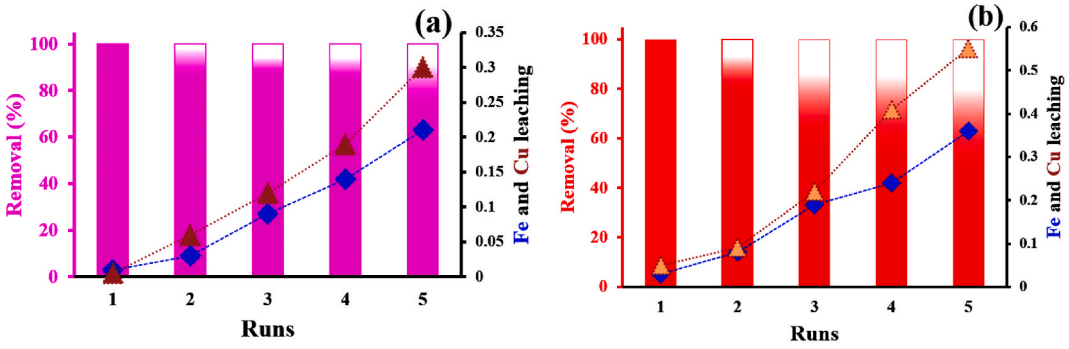

Fig. 6. a) natural b) synthetic chalcopyrite stability and reusability.

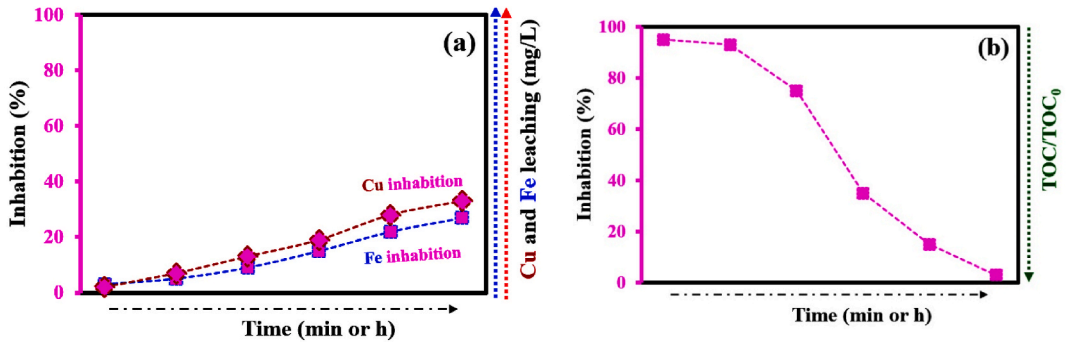

Fig. 7. Variation of toxicity of leaching metals (a) and intermediates (b).

software (Taguchi, central composite design (CCD), response surface methodology (RSM), and others) is required to achieve better degradation efficiency.

2. Even though the use of chalcopyrite-based oxidation processes has demonstrated effective degradation of pollutants, the issue of metal leaching remains a major concern, particularly in acidic conditions. Therefore, there is a need for additional efforts to reduce metal leaching and create more ecologically sustainable and environmentally friendly approaches such use of non-metal supports (biochar, carbon nanotubes, etc) and heterogeneous ternary metal oxide nanocomposites.
3. Although various mechanisms have been suggested to explain the removal of pollutants through chalcopyrite activation of oxidants, there is still an insufficient understanding of the fundamental processes involved. Therefore, further investigation is necessary to gain a complete comprehension of the degradation mechanisms and pathways associated with this process.
4. The assessment of the environmental impact of chalcopyrite-based oxidation processes is crucial. The toxicity evaluation of the Fe and Cu leaching showed that new toxic compounds were formed by recombination of some nontoxic fragments. Therefore, further research is needed to assess the potential environmental impact of these compounds and to develop methods for their removal.
5. While chalcopyrite-based oxidation processes have displayed encouraging outcomes in laboratory-scale experiments, there is a need for further research and development to scale up the processes to an industrial level.

12. Conclusion

This article discussed the use of chalcopyrite ($CuFeS_2$) as a catalyst for pollutant removal and highlights the importance of considering factors such as pH, oxidant concentration, and catalyst dosage in the degradation process. It finds that acidic conditions are more effective in pollutant degradation due to increased ROS generation, but there is high metal leaching. The study showed that chalcopyrite exhibits high catalytic activity in Fenton-based and EO processes due to its ability to provide $Fe^{2+/3+}$ and $Cu1^{+/2+}$ ions for oxidants activation and ROS generation. However, excessive catalyst dosage and oxidant concentration can lead to a decline in removal efficiency and environmental risk due to high metal leaching. Depending on the type of reaction (Fenton, photo-Fenton, electro-Fenton, etc.), different ROS including $^{\bullet}OH$, $SO_4^{\bullet -}$, $^1O_2$, $O_2^{\bullet -}$, $^{\bullet}CO_3$, $HO_2^{\bullet}$, and $R^{\bullet}$ have been involved in pollutant removal by $CuFeS_2$ activation of oxidants. Also, the $Fe^{2+/3+}$ and $Cu1^{+/2+}$ cycles are the main mechanism of the catalyst's activity. The stability and toxicity evaluations showed that the reusability of natural chalcopyrite is more effective than the synthetic type, and the recovery process affects the catalyst activity. Toxicity evaluation showed Fe and Cu leaching have toxic effects and new toxic compounds were caused by recombination of some nontoxic fragments.

Author contribution statement

All authors listed have significantly contributed to the development and the writing of this article.

Data availability statement

Data will be made available on request.

Declaration of competing interest

The authors declare that they have no known competing financial interests or personal relationships that could have appeared to influence the work reported in this paper.

Acknowledgements

Authors appreciate the financial support by the Kermanshah University of Medical Sciences (KUMS) (Grant Number: 4000946).

References

[1] W. Song, J. Li, Z. Wang, X. Zhang, A mini review of activated methods to persulfate-based advanced oxidation process, Water Sci. Technol. 79 (2019) 573–579.
[2] D.B. Miklos, C. Remy, M. Jekel, K.G. Linden, J.E. Drewes, U. Hübner, Evaluation of advanced oxidation processes for water and wastewater treatment–A critical review, Water Res. 139 (2018) 118–131.
[3] K. Liu, J. Chen, F. Sun, Y. Liu, M. Tang, Y. Yang, Historical development and prospect of intimately coupling photocatalysis and biological technology for pollutant treatment in sewage: a review, Sci. Total Environ. (2022), 155482.
[4] Z. Liu, M. He, L. Tang, B. Shao, Q. Liang, T. Wu, Y. Pan, X. Zhang, S. Luo, Q. He, Dual redox cycles of Mn (II)/Mn (III) and Mn (III)/Mn (IV) on porous Mn/N co-doped biochar surfaces for promoting peroxymonosulfate activation and ciprofloxacin degradation, J. Colloid Interface Sci. 634 (2023) 255–267.
[5] A. Tursi, M. Baratta, T. Easton, E. Chatzisymeon, F. Chidichimo, M. De Biase, G. De Filpo, Microplastics in aquatic systems, a comprehensive review: origination, accumulation, impact, and removal technologies, RSC Adv. 12 (2022) 28318–28340.
[6] M.P. Rayaroth, C.T. Aravindakumar, N.S. Shah, G. Boczkaj, Advanced oxidation processes (AOPs) based wastewater treatment-unexpected nitration side reactions-a serious environmental issue: a review, Chem. Eng. J. 430 (2022), 133002.
[7] Q. Liang, X. Liu, B. Shao, L. Tang, Z. Liu, W. Zhang, S. Gong, Y. Liu, Q. He, T. Wu, Construction of fish-scale tubular carbon nitride-based heterojunction with boosting charge separation in photocatalytic tetracycline degradation and H2O2 production, Chem. Eng. J. 426 (2021), 130831.
[8] Y. Yang, Z. Zeng, G. Zeng, D. Huang, R. Xiao, C. Zhang, C. Zhou, W. Xiong, W. Wang, M. Cheng, Ti3C2 Mxene/porous g-C3N4 interfacial Schottky junction for boosting spatial charge separation in photocatalytic H2O2 production, Appl. Catal. B Environ. 258 (2019), 117956.
[9] Z. Jiang, L. Wang, J. Lei, Y. Liu, J. Zhang, Photo-Fenton degradation of phenol by CdS/rGO/Fe2+ at natural pH with in situ-generated H2O2, Appl. Catal. B Environ. 241 (2019) 367–374.
[10] P. Zawadzki, M. Deska, Degradation efficiency and kinetics analysis of an advanced oxidation process utilizing ozone, hydrogen peroxide and persulfate to degrade the dye Rhodamine B, Catalysts 11 (2021) 974.
[11] D. Lin, Y. Fu, X. Li, L. Wang, M. Hou, D. Hu, Q. Li, Z. Zhang, C. Xu, S. Qiu, Application of persulfate-based oxidation processes to address diverse sustainability challenges: a critical review, J. Hazard Mater. 440 (2022), 129722.
[12] A. Fernandes, P. Makoś, G. Boczkaj, Treatment of bitumen post oxidative effluents by sulfate radicals based advanced oxidation processes (S-AOPs) under alkaline pH conditions, J. Clean. Prod. 195 (2018) 374–384.
[13] Z. Honarmandrad, X. Sun, Z. Wang, M. Naushad, G. Boczkaj, Activated persulfate and peroxymonosulfate based advanced oxidation processes (AOPs) for antibiotics degradation–A review, Water Resour. Ind. (2022), 100194.
[14] K. Fedorov, M.P. Rayaroth, N.S. Shah, G. Boczkaj, Activated sodium percarbonate-ozone (SPC/O3) hybrid hydrodynamic cavitation system for advanced oxidation processes (AOPs) of 1, 4-dioxane in water, J. Chem. Eng. 456 (2023), 141027.
[15] J. Lee, U. Von Gunten, J.-H. Kim, Persulfate-based advanced oxidation: critical assessment of opportunities and roadblocks, Environ. Sci. Technol. 54 (2020) 3064–3081.
[16] F. Ghanbari, M. Moradi, Application of peroxymonosulfate and its activation methods for degradation of environmental organic pollutants, J. Chem. Eng. 310 (2017) 41–62.
[17] F. Qin, E. Almatrafi, C. Zhang, D. Huang, L. Tang, A. Duan, D. Qin, H. Luo, C. Zhou, G. Zeng, Catalyst-free photochemical activation of peroxymonosulfate in xanthene-rich systems for fenton-like synergistic decontamination: efficacy of proton transfer process, Angew. Chem., Int. Ed. 62 (2023), e202300256.
[18] B. Shao, Z. Liu, L. Tang, Y. Liu, Q. Liang, T. Wu, Y. Pan, X. Zhang, X. Tan, J. Yu, The effects of biochar on antibiotic resistance genes (ARGs) removal during different environmental governance processes: a review, J. Hazard Mater. 435 (2022), 129067.
[19] Y. Ding, L. Fu, X. Peng, M. Lei, C. Wang, J. Jiang, Copper catalysts for radical and nonradical persulfate based advanced oxidation processes: certainties and uncertainties, J. Chem. Eng. 427 (2022), 131776.
[20] W.-D. Oh, Z. Dong, T.-T. Lim, Generation of sulfate radical through heterogeneous catalysis for organic contaminants removal: current development, challenges and prospects, Appl. Catal. B Environ. 194 (2016) 169–201.
[21] Y. Lei, C.-S. Chen, Y.-J. Tu, Y.-H. Huang, H. Zhang, Heterogeneous degradation of organic pollutants by persulfate activated by CuO-Fe3O4: mechanism, stability, and effects of pH and bicarbonate ions, Environ. Sci. Technol. 49 (2015) 6838–6845.
[22] Y. Bao, W.-D. Oh, T.-T. Lim, R. Wang, R.D. Webster, X. Hu, Elucidation of stoichiometric efficiency, radical generation and transformation pathway during catalytic oxidation of sulfamethoxazole via peroxymonosulfate activation, Water Res. 151 (2019) 64–74.
[23] J. Deng, Y. Shao, N. Gao, C. Tan, S. Zhou, X. Hu, CoFe2O4 magnetic nanoparticles as a highly active heterogeneous catalyst of oxone for the degradation of diclofenac in water, J. Hazard Mater. 262 (2013) 836–844.
[24] Y. Zhang, Q. Zhang, Z. Dong, J. Hong, Degradation of acetaminophen with ferrous/copperoxide activate persulfate: synergism of iron and copper, Water Res. 146 (2018) 232–243.
[25] M. He, Q. Liang, L. Tang, Z. Liu, B. Shao, Q. He, T. Wu, S. Luo, Y. Pan, C. Zhao, Advances of covalent organic frameworks based on magnetism: classification, synthesis, properties, applications, Coord. Chem. Rev. 449 (2021), 214219.
[26] L. Xu, J. Li, W. Zeng, K. Liu, Y. Ma, L. Fang, C. Shi, Surfactant-assisted removal of 2, 4-dichlorophenol from soil by zero-valent Fe/Cu activated persulfate, Chin, J. Chem. Eng. 44 (2022) 447–455.
[27] Q. Dong, H. Dong, Y. Li, J. Xiao, S. Xiang, X. Hou, D. Chu, Degradation of sulfamethazine in water by sulfite activated with zero-valent Fe-Cu bimetallic nanoparticles, J. Hazard Mater. 431 (2022), 128601.
[28] H. Weng, Y. Yang, C. Zhang, M. Cheng, W. Wang, B. Song, H. Luo, D. Qin, C. Huang, F. Qin, Insight into FeOOH-mediated advanced oxidation processes for the treatment of organic polluted wastewater, J. Chem. Eng. 453 (2023), 139812.
[29] P.-Y. Wen, T.-Y. Lai, T. Wu, Y.-W. Lin, Hydrothermal and Co-precipitated synthesis of chalcopyrite for fenton-like degradation toward rhodamine B, Catalysts 12 (2022) 152.
[30] N. Barhoumi, H. Olvera-Vargas, N. Oturan, D. Huguenot, A. Gadri, S. Ammar, E. Brillas, M.A. Oturan, Kinetics of oxidative degradation/mineralization pathways of the antibiotic tetracycline by the novel heterogeneous electro-Fenton process with solid catalyst chalcopyrite, App.Catal.B: Environ. Times 209 (2017) 637–647.
[31] S. Wang, J. Tian, Q. Wang, F. Xiao, S. Gao, W. Shi, F. Cui, Development of CuO coated ceramic hollow fiber membrane for peroxymonosulfate activation: a highly efficient singlet oxygen-dominated oxidation process for bisphenol a degradation, App.Catal.B: Environ. Times 256 (2019), 117783.
[32] A. Jawad, K. Zhan, H. Wang, A. Shahzad, Z. Zeng, J. Wang, X. Zhou, H. Ullah, Z. Chen, Z. Chen, Tuning of persulfate activation from a free radical to a nonradical pathway through the incorporation of non-redox magnesium oxide, Environ. Sci. Technol. 54 (2020) 2476–2488.
[33] A. Fernandes, P. Makoś, Z. Wang, G. Boczkaj, Synergistic effect of TiO2 photocatalytic advanced oxidation processes in the treatment of refinery effluents, J. Chem. Eng. 391 (2020), 123488.
[34] S. Xiao, M. Cheng, H. Zhong, Z. Liu, Y. Liu, X. Yang, Q. Liang, Iron-mediated activation of persulfate and peroxymonosulfate in both homogeneous and heterogeneous ways: a review, J. Chem. Eng. 384 (2020), 123265.
[35] K. Hou, Z. Pi, F. Yao, B. Wu, L. He, X. Li, D. Wang, H. Dong, Q. Yang, A critical review on the mechanisms of persulfate activation by iron-based materials: clarifying some ambiguity and controversies, J. Chem. Eng. 407 (2021), 127078.
[36] L. Labiadh, S. Ammar, A.R. Kamali, Oxidation/mineralization of AO7 by electro-Fenton process using chalcopyrite as the heterogeneous source of iron and copper catalysts with enhanced degradation activity and reusability, J. Electroanal. Chem. 853 (2019), 113532.
[37] X. Xu, D. Tang, J. Cai, B. Xi, Y. Zhang, L. Pi, X. Mao, Heterogeneous activation of peroxymonocarbonate by chalcopyrite (CuFeS2) for efficient degradation of 2, 4-dichlorophenol in simulated groundwater, App.Catal.B: Environ. Times 251 (2019) 273–282.
[38] H. Zhao, X. Huang, J. Wang, Y. Li, R. Liao, X. Wang, X. Qiu, Y. Xiong, W. Qin, G. Qiu, Comparison of bioleaching and dissolution process of p-type and n-type chalcopyrite, Miner. Eng. 109 (2017) 153–161.

[39] A.H. Ltaïef, L.M. Pastrana-Martínez, S. Ammar, A. Gadri, J.L. Faria, A.M. Silva, Mined pyrite and chalcopyrite as catalysts for spontaneous acidic pH adjustment in Fenton and LED photo-Fenton-like processes, J. Chem. Technol. Biotechnol. 93 (2018) 1137–1146.
[40] C. Droguett, R. Salazar, E. Brillas, I. Sirés, C. Carlesi, J.F. Marco, A. Thiam, Treatment of antibiotic cephalexin by heterogeneous electrochemical Fenton-based processes using chalcopyrite as sustainable catalyst, Sci. Total Environ. 740 (2020), 140154.
[41] Y. Vieira, K. da Boit Martinello, T.H. Ribeiro, J.P. Silveira, J.S. Salla, L.F. Silva, E.L. Foletto, G.L. Dotto, Photo-assisted degradation of organic pollutant by CuFeS2 powder in RGB-LED reactors: a comprehensive study of band gap values and the relation between wavelength and electron-hole recombination, Adv. Powder Technol. 33 (2022), 103368.
[42] W. Nie, Q. Mao, Y. Ding, Y. Hu, H. Tang, Highly efficient catalysis of chalcopyrite with surface bonded ferrous species for activation of peroxymonosulfate toward degradation of bisphenol A: a mechanism study, J. Hazard Mater. 364 (2019) 59–68.
[43] J. da Silveira Salla, K. da Boit Martinello, G.L. Dotto, E. García-Díaz, H. Javed, P.J. Alvarez, E.L. Foletto, Synthesis of citrate–modified CuFeS2 catalyst with significant effect on the photo–Fenton degradation efficiency of bisphenol a under visible light and near–neutral pH, Colloids Surf. A Physicochem. Eng. Asp. 595 (2020), 124679.
[44] J. da Silveira Salla, G.L. Dotto, D. Hotza, R. Landers, K. da Boit Martinello, E.L. Foletto, Enhanced catalytic performance of CuFeS2 chalcogenide prepared by microwave-assisted route for photo-Fenton oxidation of emerging pollutant in water, J. Environ. Chem. Eng. 8 (2020), 104077.
[45] S.-A. Chang, P.-Y. Wen, T. Wu, Y.-W. Lin, Microwave-assisted synthesis of chalcopyrite/silver phosphate composites with enhanced degradation of Rhodamine B under photo-Fenton process, Nanomaterials 10 (2020) 2300.
[46] A. Fernandes, P. Makoś, J.A. Khan, G. Boczkaj, Pilot scale degradation study of 16 selected volatile organic compounds by hydroxyl and sulfate radical based advanced oxidation processes, J. Clean. Prod. 208 (2019) 54–64.
[47] R. Yuan, M. Jiang, S. Gao, Z. Wang, H. Wang, G. Boczkaj, Z. Liu, J. Ma, Z. Li, 3D mesoporous α-Co (OH) 2 nanosheets electrodeposited on nickel foam: a new generation of macroscopic cobalt-based hybrid for peroxymonosulfate activation, Chem. Eng. J. 380 (2020), 122447.
[48] X. Duan, S. Yang, S. Wacławek, G. Fang, R. Xiao, D.D. Dionysiou, Limitations and prospects of sulfate-radical based advanced oxidation processes, J. Environ. Chem. Eng. 8 (2020), 103849.
[49] X. Xia, F. Zhu, J. Li, H. Yang, L. Wei, Q. Li, J. Jiang, G. Zhang, Q. Zhao, A review study on sulfate-radical-based advanced oxidation processes for domestic/industrial wastewater treatment: degradation, efficiency, and mechanism, Front. Chem. 8 (2020), 592056.
[50] S. Guerra-Rodríguez, E. Rodríguez, D.N. Singh, J. Rodríguez-Chueca, Assessment of sulfate radical-based advanced oxidation processes for water and wastewater treatment: a review, Water 10 (2018) 1828.
[51] Q. He, C. Zhao, L. Tang, Z. Liu, B. Shao, Q. Liang, T. Wu, Y. Pan, J. Wang, Y. Liu, Peroxymonosulfate and peroxydisulfate activation by fish scales biochar for antibiotics removal: synergism of N, P-codoped biochar, Chemosphere 326 (2023), 138326.
[52] R. Yuan, Z. Jiang, Z. Wang, S. Gao, Z. Liu, M. Li, G. Boczkaj, Hierarchical MnO2 nanoflowers blooming on 3D nickel foam: a novel micro-macro catalyst for peroxymonosulfate activation, J. Colloid Interface Sci. 571 (2020) 142–154.
[53] K. Fedorov, M. Plata-Gryl, J.A. Khan, G. Boczkaj, Ultrasound-assisted heterogeneous activation of persulfate and peroxymonosulfate by asphaltenes for the degradation of BTEX in water, J. Hazard Mater. 397 (2020), 122804.
[54] L. Wang, D. Luo, O. Hamdaoui, Y. Vasseghian, M. Momotko, G. Boczkaj, G.Z. Kyzas, C. Wang, Bibliometric analysis and literature review of ultrasound-assisted degradation of organic pollutants, Sci. Total Environ. 876 (2023), 162551.
[55] K. Fedorov, K. Dinesh, X. Sun, R.D.C. Soltani, Z. Wang, S. Sonawane, G. Boczkaj, Synergistic effects of hybrid advanced oxidation processes (AOPs) based on hydrodynamic cavitation phenomenon–a review, Chem. Eng. J. 432 (2022), 134191.
[56] M. Gągol, A. Przyjazny, G. Boczkaj, Wastewater treatment by means of advanced oxidation processes based on cavitation–a review, Chem. Eng. J. 338 (2018) 599–627.
[57] Y. Deng, R. Zhao, Advanced oxidation processes (AOPs) in wastewater treatment, Curr. Pollut. Rep. 1 (2015) 167–176.
[58] J.L. Wang, L.J. Xu, Advanced oxidation processes for wastewater treatment: formation of hydroxyl radical and application, Crit. Rev. Environ. Sci. Technol. 42 (2012) 251–325.
[59] A. Fernandes, M. Gągol, P. Makoś, J.A. Khan, G. Boczkaj, Integrated photocatalytic advanced oxidation system (TiO2/UV/O3/H2O2) for degradation of volatile organic compounds, Sep. Purif. Technol. 224 (2019) 1–14.
[60] X. Zhang, S. Tong, D. Huang, Z. Liu, B. Shao, Q. Liang, T. Wu, Y. Pan, J. Huang, Y. Liu, Recent advances of Zr based metal organic frameworks photocatalysis: energy production and environmental remediation, Coord. Chem. Rev. 448 (2021), 214177.
[61] M. Skipitari, E. Kalaitzopoulou, P. Papadea, A. Varemmenou, V.E. Gavriil, E. Sarantopoulou, A.-C. Cefalas, S. Tsakas, E. Rosmaraki, I. Margiolaki, Titanium dioxide nanoparticle-based hydroxyl and superoxide radical production for oxidative stress biological simulations, J. Photochem. Photobiol., A: Chem 435 (2023), 114290.
[62] T. Wu, Q. Liang, L. Tang, J. Tang, J. Wang, B. Shao, S. Gong, Q. He, Y. Pan, Z. Liu, Construction of a novel S-scheme heterojunction piezoelectric photocatalyst V-BiOIO3/FTCN and immobilization with floatability for tetracycline degradation, J. Hazard Mater. 443 (2023), 130251.
[63] J. Ran, H. Duan, C. Srinivasakannan, J. Yao, S. Yin, L. Zhang, Effective removal of organics from Bayer liquor through combined sonolysis and ozonation: kinetics and mechanism, Ultrason. Sonochem. 88 (2022), 106106.
[64] G. Zeng, M. Shi, M. Dai, Q. Zhou, H. Luo, L. Lin, K. Zang, Z. Meng, X. Pan, Hydroxyl radicals in natural waters: light/dark mechanisms, changes and scavenging effects, Sci. Total Environ. 868 (2023), 161533.
[65] Y. Li, H. Dong, L. Li, J. Xiao, S. Xiao, Z. Jin, Efficient degradation of sulfamethazine via activation of percarbonate by chalcopyrite, Water Res. 202 (2021), 117451.
[66] J. Peng, H. Zhou, W. Liu, Z. Ao, H. Ji, Y. Liu, S. Su, G. Yao, B. Lai, Insights into heterogeneous catalytic activation of peroxymonosulfate by natural chalcopyrite: pH-dependent radical generation, degradation pathway and mechanism, Chem. Eng. J. 397 (2020), 125387.
[67] X. Huang, T. Zhu, W. Duan, S. Liang, G. Li, W. Xiao, Comparative studies on catalytic mechanisms for natural chalcopyrite-induced Fenton oxidation: effect of chalcopyrite type, J. Hazard Mater. 381 (2020), 120998.
[68] J. Yang, R. Huang, Y. Cao, H. Wang, A. Ivanets, C. Wang, Heterogeneous Fenton degradation of persistent organic pollutants using natural chalcopyrite: effect of water matrix and catalytic mechanism, Environ. Sci. Pollut. Res. 29 (2022) 75651–75663.
[69] Y. Vieira, M.B. Ceretta, E.L. Foletto, E.A. Wolski, S. Silvestri, Application of a novel rGO-CuFeS2 composite catalyst conjugated to microwave irradiation for ultra-fast real textile wastewater treatment, J. Water Process Eng. 36 (2020), 101397.
[70] G. Xi, S. Chen, X. Zhang, Y. Xing, Z. He, Insights into the Degradation of Carbamazepine by Persulfate Activated by Chalcopyrite: Degradation Mechanism and Synergy with Zero-Valent Iron, 2022.
[71] Y. Ding, Y. Ruan, L. Zhu, H. Tang, Efficient oxidative degradation of chlorophenols by using magnetic surface carboxylated Cu0/Fe3O4 nanocomposites in a wide pH range, J. Environ. Chem. Eng. 5 (2017) 2681–2690.
[72] Y. Zhang, H.P. Tran, I. Hussain, Y. Zhong, S. Huang, Degradation of p-chloroaniline by pyrite in aqueous solutions, Chem. Eng. J. 279 (2015) 396–401.
[73] H.T. Pham, M. Kitsuneduka, J. Hara, K. Suto, C. Inoue, Trichloroethylene transformation by natural mineral pyrite: the deciding role of oxygen, Environ. Sci. Technol. 42 (2008) 7470–7475.
[74] M. Khabbaz, M.H. Entezari, Degradation of Diclofenac by sonosynthesis of pyrite nanoparticles, J. Environ. Manag. 187 (2017) 416–423.
[75] L. Kong, X. Hu, M. He, Mechanisms of Sb (III) oxidation by pyrite-induced hydroxyl radicals and hydrogen peroxide, Environ. Sci. Technol. 49 (2015) 3499–3505.
[76] X. Zang, X. Gu, S. Lu, Z. Miao, X. Zhang, X. Fu, G.Y. Fu, Z. Qiu, Q. Sui, Enhanced degradation of trichloroethene by sodium percarbonate activated with Fe (II) in the presence of citric acid, Water Sci. Technol. Water Supply 17 (2017) 665–673.
[77] X. Fu, X. Gu, S. Lu, V.K. Sharma, M.L. Brusseau, Y. Xue, M. Danish, G.Y. Fu, Z. Qiu, Q. Sui, Benzene oxidation by Fe (III)-activated percarbonate: matrix-constituent effects and degradation pathways, Chem. Eng. J. 309 (2017) 22–29.

[78] P. Yan, Q. Sui, S. Lyu, H. Hao, H.F. Schröder, W. Gebhardt, Elucidation of the oxidation mechanisms and pathways of sulfamethoxazole degradation under Fe (II) activated percarbonate treatment, Sci. Total Environ. 640 (2018) 973–980.
[79] S. Wang, J. Wu, X. Lu, W. Xu, Q. Gong, J. Ding, B. Dan, P. Xie, Removal of acetaminophen in the Fe2+/persulfate system: kinetic model and degradation pathways, Chem. Eng. J. 358 (2019) 1091–1100.
[80] H. Yang, S. Zhuang, Q. Hu, L. Hu, L. Yang, C. Au, B. Yi, Competitive reactions of hydroxyl and sulfate radicals with sulfonamides in Fe2+/S2O82− system: reaction kinetics, degradation mechanism and acute toxicity, Chem. Eng. J. 339 (2018) 32–41.
[81] S. Wang, J. Wang, Trimethoprim degradation by Fenton and Fe (II)-activated persulfate processes, Chemosphere 191 (2018) 97–105.
[82] R. Pulicharla, R. Drouinaud, S.K. Brar, P. Drogui, F. Proulx, M. Verma, R.Y. Surampalli, Activation of persulfate by homogeneous and heterogeneous iron catalyst to degrade chlortetracycline in aqueous solution, Chemosphere 207 (2018) 543–551.
[83] X. Pan, L. Yan, R. Qu, Z. Wang, Degradation of the UV-filter benzophenone-3 in aqueous solution using persulfate activated by heat, metal ions and light, Chemosphere 196 (2018) 95–104.
[84] M. Zhang, X. Chen, H. Zhou, M. Muruganantha, Y. Zhang, Degradation of p-nitrophenol by heat and metal ions co-activated persulfate, Chem. Eng. J. 264 (2015) 39–47.
[85] T. Cai, L. Bu, Y. Wu, S. Zhou, Z. Shi, Accelerated degradation of bisphenol A induced by the interaction of EGCG and Cu (II) in Cu (II)/EGCG/ peroxymonosulfate process, Chem. Eng. J. 395 (2020), 125134.
[86] H. Chi, X. He, J. Zhang, D. Wang, X. Zhai, J. Ma, Hydroxylamine enhanced degradation of naproxen in Cu2+ activated peroxymonosulfate system at acidic condition: efficiency, mechanisms and pathway, Chem. Eng. J. 361 (2019) 764–772.
[87] R. Wang, H. An, H. Zhang, X. Zhang, J. Feng, T. Wei, Y. Ren, High active radicals induced from peroxymonosulfate by mixed crystal types of CuFeO2 as catalysts in the water, Appl. Surf. Sci. 484 (2019) 1118–1127.
[88] Y. Ren, L. Lin, J. Ma, J. Yang, J. Feng, Z. Fan, Sulfate radicals induced from peroxymonosulfate by magnetic ferrospinel MFe2O4 (M= Co, Cu, Mn, and Zn) as heterogeneous catalysts in the water, Appl. Catal. B Environ. 165 (2015) 572–578.
[89] J. Li, Y. Ren, F. Ji, B. Lai, Heterogeneous catalytic oxidation for the degradation of p-nitrophenol in aqueous solution by persulfate activated with CuFe2O4 magnetic nano-particles, Chem. Eng. J. 324 (2017) 63–73.
[90] Y. Ding, L. Zhu, N. Wang, H. Tang, Sulfate radicals induced degradation of tetrabromobisphenol A with nanoscaled magnetic CuFe2O4 as a heterogeneous catalyst of peroxymonosulfate, Appl. Catal. B Environ. 129 (2013) 153–162.
[91] Y.-H. Guan, J. Ma, Y.-M. Ren, Y.-L. Liu, J.-Y. Xiao, L.-q. Lin, C. Zhang, Efficient degradation of atrazine by magnetic porous copper ferrite catalyzed peroxymonosulfate oxidation via the formation of hydroxyl and sulfate radicals, Water Res. 47 (2013) 5431–5438.
[92] Q. Peng, Y. Ding, L. Zhu, G. Zhang, H. Tang, Fast and complete degradation of norfloxacin by using Fe/Fe3C@ NG as a bifunctional catalyst for activating peroxymonosulfate, Sep. Purif. Technol. 202 (2018) 307–317.
[93] Y. Wang, H. Sun, H.M. Ang, M.O. Tadé, S. Wang, Facile synthesis of hierarchically structured magnetic MnO2/ZnFe2O4 hybrid materials and their performance in heterogeneous activation of peroxymonosulfate, ACS Appl. Mater. Interfaces 6 (2014) 19914–19923.
[94] Y. Wu, Y. Li, H. Wang, Soil Decontamination by Natural Minerals via Fenton-Like Reactions: A Comparison Study of Chalcopyrite and Pyrite, Available at: SSRN 4268926..
[95] L. Li, Y. Zhang, S. Yang, S. Zhang, Q. Xu, P. Chen, Y. Du, Y. Xing, Cobalt-loaded cherry core biochar composite as an effective heterogeneous persulfate catalyst for bisphenol A degradation, RSC Adv. 12 (2022) 7284–7294.
[96] D. Hou, X. Hu, W. Ho, P. Hu, Y. Huang, Facile fabrication of porous Cr-doped SrTiO 3 nanotubes by electrospinning and their enhanced visible-light-driven photocatalytic properties, J. Mater. Chem. A 3 (2015) 3935–3943.
[97] A. Gupta, J.R. Saurav, S. Bhattacharya, Solar light based degradation of organic pollutants using ZnO nanobrushes for water filtration, RSC Adv. 5 (2015) 71472–71481.
[98] M. Moradi, A. Elahinia, Y. Vasseghian, E.-N. Dragoi, F. Omidi, A.M. Khaneghah, A review on pollutants removal by Sono-photo-Fenton processes, J. Environ. Chem. Eng. 8 (2020), 104330.
[99] M. Umar, H.A. Aziz, M.S. Yusoff, Trends in the use of Fenton, electro-Fenton and photo-Fenton for the treatment of landfill leachate, Waste Manag. 30 (2010) 2113–2121.
[100] Z. Li, J. Chen, C. Wang, J. Zhao, Q. Wei, X. Ma, G. Yang, Study on the removal and degradation mechanism of microcystin-LR by the UV/Fenton system, Sci. Total Environ. (2023), 164665.
[101] N. Thomas, D.D. Dionysiou, S.C. Pillai, Heterogeneous Fenton catalysts: a review of recent advances, J. Hazard Mater. 404 (2021), 124082.
[102] C. Wang, J. Ye, L. Liang, X. Cui, L. Kong, N. Li, Z. Cheng, W. Peng, B. Yan, G. Chen, Application of MXene-based materials in Fenton-like systems for organic wastewater treatment: a review, Sci. Total Environ. 862 (2023), 160539.
[103] A.J. Dos Santos, I. Sirés, A.P. Alves, C.A. Martínez-Huitle, E. Brillas, Vermiculite as heterogeneous catalyst in electrochemical Fenton-based processes: application to the oxidation of Ponceau SS dye, Chemosphere 240 (2020), 124838.
[104] D.F. Laine, I.F. Cheng, Analysis of hydrogen peroxide and an organic hydroperoxide via the electrocatalytic Fenton reaction, Microchem. J. 91 (2009) 78–81.
[105] C. Bruguera-Casamada, R.M. Araujo, E. Brillas, I. Sires, Advantages of electro-Fenton over electrocoagulation for disinfection of dairy wastewater, Chem. Eng. J. 376 (2019), 119975.
[106] D. Gümüş, F. Akbal, Comparison of Fenton and electro-Fenton processes for oxidation of phenol, Process Saf. Environ. Protect. 103 (2016) 252–258.
[107] J. Wang, S. Wang, Toxicity changes of wastewater during various advanced oxidation processes treatment: an overview, J. Clean. Prod. 315 (2021), 128202.